Environmental Research 135 (2014) 204–211

Contents lists available at ScienceDirect

Environmental Research

journal homepage: www.elsevier.com/locate/envres

A national satellite-based land-use regression model for air pollution exposure assessment in Australia

Luke D. Knibbs [a,*], Michael G. Hewson [b], Matthew J. Bechle [c], Julian D. Marshall [c], Adrian G. Barnett [d]

[a] School of Population Health, The University of Queensland, Brisbane, Australia
[b] School of Geography, Planning and Environmental Management, The University of Queensland, Brisbane, Australia
[c] Department of Civil Engineering, The University of Minnesota, Minneapolis, USA
[d] School of Public Health and Social Work & Institute of Health and Biomedical Innovation, Queensland University of Technology, Brisbane, Australia

ARTICLE INFO

Article history:
Received 26 June 2014
Received in revised form
16 September 2014
Accepted 18 September 2014

Keywords:
Nitrogen dioxide
Land use regression
Exposure
Epidemiology
Australia

ABSTRACT

Land-use regression (LUR) is a technique that can improve the accuracy of air pollution exposure assessment in epidemiological studies. Most LUR models are developed for single cities, which places limitations on their applicability to other locations. We sought to develop a model to predict nitrogen dioxide (NO_2) concentrations with national coverage of Australia by using satellite observations of tropospheric NO_2 columns combined with other predictor variables. We used a generalised estimating equation (GEE) model to predict annual and monthly average ambient NO_2 concentrations measured by a national monitoring network from 2006 through 2011. The best annual model explained 81% of spatial variation in NO_2 (absolute RMS error = 1.4 ppb), while the best monthly model explained 76% (absolute RMS error = 1.9 ppb). We applied our models to predict NO_2 concentrations at the ~350,000 census mesh blocks across the country (a mesh block is the smallest spatial unit in the Australian census). National population-weighted average concentrations ranged from 7.3 ppb (2006) to 6.3 ppb (2011). We found that a simple approach using tropospheric NO_2 column data yielded models with slightly better predictive ability than those produced using a more involved approach that required simulation of surface-to-column ratios. The models were capable of capturing within-urban variability in NO_2, and offer the ability to estimate ambient NO_2 concentrations at monthly and annual time scales across Australia from 2006–2011. We are making our model predictions freely available for research.

1. Introduction

Outdoor (ambient) air pollution is a major contributor to the global burden of disease and a leading environmental risk factor for morbidity and mortality (Lim et al., 2012). Accurate estimates of people's exposure to ambient air pollution are required to quantify and understand its effects on health. Exposure estimates have traditionally involved using average measurements from air pollution monitors (e.g. Barnett et al., 2005), assigning exposure using the nearest monitor to a person's residence (e.g. Ritz et al., 2002) or using a proxy like distance to the nearest main road (e.g. Hoffmann et al., 2007). There is potential for exposure misclassification with all these approaches due to their limited ability to capture the spatial variability that characterises some air pollutants (Jerrett et al., 2005; Hoek et al., 2008).

Land-use regression (LUR) is a technique that can improve the accuracy of air pollution exposure estimates. It uses measurements at a set of locations combined with spatial variables to build statistical models that can predict concentrations at unmeasured locations (Hoek et al., 2008). A key limitation of most LUR models is that they are constrained to individual cities, and a model built for one location is not necessarily transferrable to another (Briggs, 2007; Vienneau et al., 2010). However, the recent availability of high quality satellite data has helped address these issues by permitting better representation of large areas in LUR. Satellite-based LUR models for the USA (Novotny et al., 2011), Canada (Hystad et al., 2011) and Western Europe (Vienneau et al., 2013) have been developed, and have similar predictive ability to city models but with national coverage. In some cases, their spatial resolution can rival that of city models (Novotny et al., 2011). These satellite-based LUR models have attractive applications in air pollution epidemiology, environmental justice, and planning studies.

* Corresponding author.
E-mail address: l.knibbs@uq.edu.au (L.D. Knibbs).

http://dx.doi.org/10.1016/j.envres.2014.09.011
0013-9351/

Australia (population ~23 million) is one of the world's least densely populated countries (3 people/km^2) but also one of the most urbanised, as ninety percent of the population live in or near cities (Australian Bureau of Statistics, 2013a,b). There are relatively few regulatory air pollution monitoring sites in Australia. For example, Canada's population is about 50% larger than Australia's, but Canada has about twice the number of monitors (Hystad et al., 2011). Most monitoring sites in Australia are located in and around major cities but are sparsely distributed, which means they are less than ideal for assessing spatial variability in ambient air pollution levels. This can make exposure assessment for the Australian population problematic.

We sought to develop a satellite-based LUR model for Australia that could predict ambient air pollution exposure levels with good accuracy. We aimed to add to the evidence base by investigating the utility of a national satellite-based LUR in a location where ground-based monitors are scant. Most previous national LUR models have focussed on annual concentrations (e.g. Hystad et al., 2011; Vienneau et al., 2013). We aimed to expand the temporal component of our models to include monthly concentrations. Having monthly estimates of exposure would be useful for examining health outcomes where exposures within the year are important (such as birth outcomes), and to examine the potential health effects of interactions between seasons and pollution exposure. We sought to produce both monthly and annual exposure estimates over a 6 year period.

2. Methods

2.1. Variables

2.1.1. Measured NO_2

We focussed on nitrogen dioxide (NO_2) because it is strong marker of traffic and other combustion-derived pollution (e.g. industry, airports) and a key component of ambient air pollution (Briggs et al., 1997; Richter et al., 2005). We obtained hourly average ground-level NO_2 measurements from January 2006 to December 2011 from the Australian agencies responsible for regulatory ambient air pollution monitoring. NO_2 concentrations were measured using the standard chemiluminescence method, which can be subject to bias due to interference by other nitrogen oxides but is widely used in research and assessing compliance with regulations (Novotny et al., 2011). The measurements had undergone basic quality assurance procedures and we examined them further for completeness and validity. There were 68 monitoring sites across Australia where NO_2 was measured during the study period (supplement, Table S3). The sites' locations ranged from dense urban areas with multiple pollution sources nearby through to rural areas with few local sources.

2.1.2. Land use

We sourced data on natural and anthropogenic features that have a plausible association with measured NO_2 concentrations. Our choice of variables was guided by previous satellite LUR models and data availability (Hystad et al., 2011; Novotny et al., 2011; Vienneau et al., 2013). The variables selected are summarised in Table 1. We incorporated land use data from a range of sources including satellites and the Australian census. Detailed information on data sources is provided in the supplement (Table S2). We used ArcGIS version 10.0 (ESRI Inc., Redlands, USA) to process our data.

2.1.3. Satellite data: NO_2

The Ozone Monitoring Instrument (OMI) aboard the Aura satellite produces daily global observations of NO_2 tropospheric column abundance at a resolution of 13×24 km^2 (nadir) using a differential optical absorption spectroscopy (DOAS) algorithm (Levelt et al., 2006). We obtained the average tropospheric NO_2 columns over Australia for each month from 2006–2011. We then produced estimates of ground-level NO_2 by using the Weather Research and Forecasting model (WRF-Chem) to predict monthly surface-to-column ratios. This approach is a standard method to convert tropospheric column NO_2 abundance (in molecules per cm^2) to ground-level NO_2 concentration (in ppb), and has been described extensively (Lamsal et al., 2008; Bechle et al., 2013). Detailed information on satellite data retrieval and processing is given in the supplement (pages S3–S9).

2.2. Modelling approach

We generated 22 buffers from 100 m to 10 km around each monitoring site (Table 1). This approach was analogous to other national-scale models and aims to capture both proximate and more distant sources of variability in NO_2 concentrations (Novotny et al., 2011; Vienneau et al., 2013). Some variables were calculated within each buffer (e.g., percent tree cover, road length, impervious surface area) using either the average or sum of the variable in each of the 22 buffers (Table 1). Other variables were determined at each monitoring point (e.g., elevation, distance to coast). Detailed information about each variable is presented in the supplement (Table S2). There were 286 buffer variables (13 variables calculated at 22 buffers each) and 29 point variables, giving a total of 315 independent variables.

2.2.1. Annual model

The dependent variable (measured NO_2) was longitudinal, as measurements were repeated at the 68 monitoring sites over 6 years. We only included years where more than 90% of the daily measurements from a site were non-missing. Selecting the best subset of predictor variables was complex as there were 315 to

Table 1
Independent variables used to build the models. Additional information on data sources and processing is presented in the supplement.

Variable (units)	**Resolution**	**Point or buffer**[a]
OMI ground-level NO_2 (ppb)	13×24 km^2 (nadir)	Point
OMI tropospheric NO_2 column density (molecules $\times 10^{15}$ / cm^2)	13×24 km^2 (nadir)	Point
Elevation (m)	30 m	Point
Distance to coast (km)	–	Point
Annual and seasonal mean rainfall (mm)	2.5 km	Point
Annual and seasonal mean daily average temperature (°C)	2.5 km	Point
Annual and seasonal mean daily solar exposure (MJ/m^2)	5 km	Point
Tree cover (%)	250 m	Buffer[b]
Impervious surfaces (%)	1 km	Buffer[b]
Major roads (km)	–	Buffer[c]
Minor roads (km)	–	Buffer[c]
Total roads (=major roads+minor roads)	–	Buffer[c]
Population density (persons/km^2)	Mesh block[d]	Buffer[b]
Land use by type (%)[e]	Mesh block[d]	Buffer[b]
Non-vehicle point source NO_X emissions (kg/yr)[f]	–	Buffer[c]
Airport (present/not present)	–	Buffer

[a] 22 Circular buffers were created with radii of 100 m, 200 m, 300 m, 400 m, 500 m, 600 m, 700 m, 800 m, 1000 m, 1200 m, 1500 m, 1800 m, 2000 m, 2500 m, 3000 m, 3500 m, 4000 m, 5000 m, 6000 m, 7000 m, 8000 m, and 10,000 m (Novotny et al., 2011).
[b] Average of variable in buffer.
[c] Sum of variable in buffer.
[d] A mesh block is the smallest spatial unit used in the Australian census and their size varies - on average they contain 62 people.
[e] Four land use categories were examined – residential, commercial, industrial, and open space (which was the sum of water, parks and agricultural land (Rose et al., 2011)).
[f] The average density (sites/km^2) of point source NO_X emissions in each buffer was also used in model building.

choose from. Because of the large number of variables and the computational issues this presented, we employed a two-stage variable selection procedure. In the first stage, we narrowed the list of variables by using the lasso method in the 'glmnet' library (Friedman et al., 2010). This places a bound on the sum of absolute coefficient values and minimises the sum of squared errors (Tibshirani, 1996). Because this method is not suitable for longitudinal data, we ran separate lasso models for each year. We tabulated the frequencies of selected variables as an indicator of their relative importance over the 6 years (supplement, pages S16–S17). We then used all those variables that were selected at least once in the second stage of variable selection.

In the second stage of variable selection we followed the general approach of Su et al. (2009). This is a forward selection procedure where an independent variable can be added to the model on the conditions that: (1) it is statistically significant at the 5% level; (2) the variance inflation factors of all variables in the model remain below five. The second condition is an attempt to avoid co-linearity. For all variables that met these two conditions, we used 10-fold cross-validation with 3 replications using the 'cvTools' library (Alfons, 2012) to choose the variable with the smallest cross-validated root mean square error. We only added a variable to the model if the mean cross-validated error plus the cross-validated standard error was smaller than the previous minimum root mean square error. This criterion aims to create a parsimonious model. These longitudinal models used all available years of data and were fitted by a generalised estimating equation (GEE) model using the 'geepack' library (Højsgaard et al., 2006). This produced one model for predicting annual average concentrations for each year during 2006–2011. We assumed an independent correlation structure for residuals from the same monitoring site.

2.2.2. Model validation

We visually checked the residuals of the final models for outliers, and used Cook's distance and df-beta statistics to test for influential observations. We used five-fold cross-validation with five replications to estimate the prediction error of the final models on an absolute and percentage scale. We examined the importance of individual sites by comparing those with the highest Cook's distance against 3 randomly selected sites (supplement, pages S20–S21). Additional details on model validation are given in the supplement (pages S13–S14). All modelling was performed using R version 3.0.3 (R Foundation for Statistical Computing, Vienna, Austria).

2.2.3. Monthly model

We used the same approach for our monthly model, except in this case there were up to 72 average concentrations for each monitoring site (12 months by 6 years). We only included months from sites where 25 or more daily pollution measurements were non-missing. The first variable selection stage using the lasso method was run separately for each month. We then used all those variables that were selected 6 or more times in the second stage. We started the second stage variable selection with a model that included month as a factor, as we strongly suspected that this would be an important variable and wanted to avoid potential proxies for month (e.g., solar radiation, rainfall, temperature) being selected unnecessarily. Using the same GEE approach as the annual model, we produced one model for predicting the 72 monthly average concentrations during 2006–2011.

2.2.4. Comparison of different satellite NO_2 estimates

We assessed whether surface NO_2 estimates derived using surface-to-column ratios from WRF-Chem lead to models with better predictive ability for ground level NO_2 than the easier to obtain estimates of tropospheric NO_2 column density. For both our annual and monthly models, we examined two alternatives; one with surface NO_2 estimates as a candidate variable ('surface model') and one with NO_2 column density estimates ('column model'). All other candidate variables were the same across the two models.

2.2.5. Applying the models

We obtained the boundaries of the ~350,000 Australian Bureau of Statistics 'mesh blocks' that cover the entirety of Australia (Australian Bureau of Statistics, 2011). Mesh blocks are the smallest spatial unit used in the Australian census. They contain 62 people on average (range 0–2339), and have a highly variable size (range: 1.0×10^{-4}–1.7×10^{5} km^2; population-weighted mean size = 26.3 km^2). The majority of populated mesh blocks include between 30 and 60 dwellings (Australian Bureau of Statistics, 2013c). We determined the centroid of every mesh block and used our final models to predict annual average NO_2 concentrations at the centroids for each year during 2006–2011 (Hystad et al., 2011; Novotny et al., 2011).

3. Results

The number of air quality monitoring sites that met the inclusion criteria for the annual model ranged from 55 (2006) to 66 (2010) out of a possible 68. There were 358 annual measurements that met the inclusion criteria over the 6-year study period. Between 47 (February 2006) and 67 (May/July 2010) out of 68 sites met the inclusion criteria for the monthly model, and there were 4371 monthly measurements over the 72 months. The descriptive statistics of measurements used to build the annual and monthly models are shown in Table 2.

The best annual surface model (i.e. model that included surface estimates of NO_2) was capable of explaining 79% of the variability in measured NO_2 concentrations (Table 3). This increased to 81% in the best annual column model (i.e. model that included tropospheric column NO_2 density). The two models had comparable absolute and percentage root mean squared (RMS) prediction errors (Table 3). All other variables in the final models were identical with the exception of summertime mean daily solar exposure, which appeared in the surface model but not the column model. In both models, the three variables that made the largest contribution to overall R^2 were satellite NO_2, impervious surfaces within 1200 m, and major roads within 500 m.

The best monthly model that included NO_2 surface estimates explained 73% of the variability in measured NO_2 (Table 4). The best model including NO_2 column measurements explained 76%. The monthly surface and column models had very similar RMS prediction errors (Table 4). Excluding year and month, there were 4 common variables that were in both monthly models (minor roads within 8000 m, major roads within 100 m, industrial site density within 400 m, industrial land use within 10,000 m). In both models, the variable that made the largest contribution to R^2 was satellite NO_2 (Table 4). The next largest contributors to the column model were minor roads within 8000 m and industrial land use within 10,000 m. The next largest contributors to the surface model were the months of July and August, which is during the Australian winter.

Residuals were approximately normally distributed in all models (supplement, Figs. S3–S6). For a given variable in the final models some monitoring sites were more influential than others, but after investigation we found no overt undue influence on the models. The results of model checking using df-beta statistics and Cook's distance are presented in the supplement (pages S18–S26). We compared the values of predictors at the monitoring sites with those at the ~350,000 mesh block centroids around Australia and found that they were very similar (supplement, Table S11).

The average NO_2 concentration predicted by the annual surface model for 2008 is in Fig. 1, which was selected as a representative example from the 6-year study period. The mostly unpopulated interior of the country had concentrations around 2 ppb. Areas with higher concentrations (from ~5 up to >20 ppb) are the

Table 2
Descriptive statistics for monitors that met the inclusion criteria for the annual and monthly models.

Model (*n* observations)	NO_2 concentration (ppb)					
	Minimum	25th	Median	Mean	75th	Maximum
Annual (358)	1.3	4.9	6.6	7.1	9.0	17.8
Monthly (4371)	0.2	4.2	6.3	7.1	9.3	27.1

Table 3
Summary of the best annual models using surface and tropospheric column NO_2 estimates. Variables are listed in order of decreasing contribution to the model's predictive ability.

Model	Variable	Units	β[a]	SE	*p*-value	R^2 decrease (%)[b]	VIF
Best annual model: surface NO_2	Intercept	ppb	13.0	2.187	< 0.001		
R^2 = 0.79	Major roads (500 m)	km	0.900	0.185	< 0.001	4.8	1.3
Absolute RMS error = 1.35 ppb	OMI surface NO_2	ppb	2.067	0.508	< 0.001	3.4	1.6
Percent RMS error [c] = 19.0 %	Impervious surfaces (1,200 m)	%	0.609	0.196	0.002	3.1	2.5
	Summertime mean daily solar exposure	MJ/m^2	−0.283	0.078	< 0.001	2.6	1.4
	Industrial NO_X emission site density (1000 m)	sites/km^2	4.096	1.143	< 0.001	2.5	1.3
	Industrial NO_X emission site density (400 m)	sites/km^2	2.585	0.242	< 0.001	2.1	1.1
	Open space (10,000 m)	%	−0.260	0.082	0.002	1.8	2.6
	Industrial land use (10,000 m)	%	0.491	0.157	0.002	1.0	1.3
	Year	Calendar year	−0.163	0.036	< 0.001	0.8	1.0
Best annual model: column NO_2	Intercept	ppb	4.563	0.515	< 0.001		
R^2 = 0.81	OMI column NO_2	molecules × $10^{15}/cm^2$	1.203	0.178	< 0.001	10	1.3
Absolute RMS error = 1.36 ppb	Impervious surfaces (1200 m)	%	0.701	0.196	< 0.001	4.3	2.4
Percent RMS error[c] = 19.1 %	Major roads (500 m)	km	0.828	0.197	< 0.001	4.1	1.3
	Industrial NO_X emission site density (1000 m)	sites/km^2	4.083	1.228	< 0.001	2.4	1.3
	Industrial NO_X emission site density (400 m)	sites/km^2	2.629	0.256	< 0.001	2.2	1.1
	Open space (10,000 m)	%	−0.170	0.074	0.021	1.0	2.1
	Industrial land use (10,000 m)	%	0.451	0.169	0.008	0.9	1.3
	Year	calendar year	−0.140	0.034	< 0.001	0.6	1.0

[a] Some variables were centred and standardised to make their parameter estimates more interpretable (see supplement);
[b] The unit decrease in model R^2 (%) when a variable is excluded. Variables that contribute more predictive ability lead to larger decreases when they are excluded.
[c] Percent RMS error is the overall average across the monitoring sites. Note: SE = standard error; VIF = variance inflation factor; RMS = root mean squared; ppb = parts per billion.

cities and major towns. The inset of Fig. 1 focuses on Sydney, Australia's most populous city (4.5 million). Elevated concentrations (> 10 ppb) were predicted on and near major roads. Maximum concentrations (> 20 ppb) were predicted in locations with many nearby major roads and industrial areas. This general pattern was present in the 8 state and territory capital cities around Australia, although levels were highest in the 3 largest cities: Sydney, Melbourne (4 million) and Brisbane (2.1 million).

The annual NO_2 concentrations predicted at the ~350,000 census mesh block centroids by our annual surface model are shown in Fig. 2 (Hart et al., 2009). The median concentration predicted across Australia decreased from 6.3 ppb in 2006 to 5.3 ppb in 2011, which was a reduction of 16% over the 6 years. Because about 25% of mesh blocks are uninhabited, we also calculated population-weighted concentrations to indicate the average concentration that Australians are exposed to. These ranged from 7.3 ppb (2006) to 6.3 ppb (2011), a decrease of 14% from 2006 to 2011. The NO_2 levels predicted at each mesh block by the column model were almost identical to those predicted by the surface model (supplement, Table S12).

We also examined predicted NO_2 concentrations in Sydney. Across the ~57,000 mesh blocks that made up the greater Sydney area (Australian Bureau of Statistics, 2011), the population-weighted average annual NO_2 concentration ranged from 9.9 ppb (2006) to 8.7 ppb (2011), a decrease of 12% between 2006 and 2011. A range of statistics on predicted NO_2 levels across Sydney are in the supplement (Table S13).

4. Discussion

We assessed the ability of satellite-based LUR models to predict monthly and annual average NO_2 concentrations in Australia from 2006–11. We found that the best annual model explained 81% of variation in NO_2, while the best monthly model explained 76%. We applied our models to predict NO_2 concentrations at each of the ~350,000 census mesh blocks across the country and found a slight but consistent decrease between 2006 and 2011. Predicted concentrations were generally modest compared to studies in the USA and Europe (Beelen et al., 2007; Hart et al., 2009; Vienneau et al., 2013), but were more comparable with those predicted in Canada using similar methods (Hystad et al., 2011).

While it is difficult to comprehensively compare our results to other national satellite-based LUR due to differences in methodology, we found that our models captured a similar or slightly higher amount of variability in NO_2. An annual model for the USA explained 78% of variability in measured NO_2, while a Canadian model explained 73% (Hystad et al., 2011; Novotny et al., 2011). A recent model covering Western Europe explained 60% of measured NO_2 variability (Vienneau et al., 2013). The prediction error of all our models was comparable or slightly lower than other studies, albeit using different validation methods (Novotny et al., 2011; Vienneau et al., 2013; Lee and Koutrakis, 2014).

The variables in our models were generally consistent with those reported in previous studies, with both major and minor roads featuring prominently as well as impervious surface cover (Novotny et al., 2011; Vienneau et al., 2013). Increased roads, impervious surfaces and industrial variables were all associated with higher NO_2. Road traffic is a major source of NO_2, and impervious surfaces are greater in built-up locations and may reflect increased NO_2 sources in these areas. Increased open space (e.g. parklands) and summertime solar exposure were both associated with lower NO_2. Open spaces are relatively free of substantial NO_2 sources, while the presence of summertime solar exposure in the annual surface model may be due to the shorter lifetime of nitrogen oxides in the lower troposphere during the summer months (Lamsal et al., 2010).

Industrial land use and the density of nearby industrial point source NO_X emissions featured in all of our models. Industrial sources are a leading contributor to outdoor NO_X in Australia (Australian Bureau of Statistics, 2012), and the conspicuous presence of industrial variables in our models is in keeping with this. Industrial emissions and industrial land use have been found to be significant predictors of NO_2 in some other national LUR models (Hart et al., 2009; Hystad et al., 2011). Including industrial variables can improve model performance but creates models that are less specific to vehicle emissions (e.g. Novotny et al., 2011). However, it also means that model predictions are able to capture

Table 4
Best monthly models using surface and tropospheric column NO_2 estimates. Variables are listed in order of decreasing contribution to the model's predictive ability.

Model	Variable	Units	β[a]	SE	*p*-value	R^2 decrease (%)[b]	VIF
Best monthly model: surface NO_2	Intercept	ppb	3.304	0.269	< 0.001		
R^2 = 0.73	OMI surface NO_2	ppb	2.244	0.336	< 0.001	5.0	1.6
Absolute RMS error = 2.02 ppb	Aug	calendar month	3.582	0.278	< 0.001	3.5	1.9
Percent RMS error[c] = 28.4 %	Jul		3.464	0.324	< 0.001	3.2	2.0
	Jun		3.323	0.356	< 0.001	2.8	2.0
	May		3.214	0.336	< 0.001	2.6	2.1
	Minor roads (8000 m)	km	1.509	1.179	< 0.001	2.5	2.2
	Major roads (100 m)	km	4.086	0.199	< 0.001	1.9	1.3
	Industrial NO_X emission site density (400 m)	sites/km^2	2.736	0.447	< 0.001	1.8	1.1
	Impervious surfaces (500 m)	%	0.530	0.204	0.009	1.6	2.4
	Sep		2.338	0.208	< 0.001	1.5	1.8
	Apr		2.157	0.206	< 0.001	1.3	1.9
	Industrial land use (10,000 m)	%	0.599	0.754	0.001	1.1	1.3
	Oct		1.596	0.138	< 0.001	0.7	1.8
	Industrial NO_X emission site density (1000 m)	sites/km^2	2.872	0.187	0.015	0.7	1.4
	Year	calendar year	-0.162	0.033	< 0.001	0.5	1.0
	Mar		1.233	0.096	< 0.001	0.4	1.8
	Nov		0.780	0.090	< 0.001	0.2	1.8
	Jan		−0.124	0.067	0.066	0.0	1.8
	Feb		0.244	0.065	< 0.001	0.0	1.8
Best monthly model: column NO_2	Intercept	ppb	2.710	0.280	< 0.001		
R^2 = 0.76	OMI column NO_2	molecules × 10^{15}/cm^2	1.182	0.139	< 0.001	8.7	1.5
Absolute RMS error = 1.93 ppb	Minor roads (8000 m)	km	1.954	0.398	< 0.001	5.6	1.7
Percent RMS error[c] = 27.1 %	Industrial land use (10,000 m)	%	1.004	0.165	< 0.001	3.2	1.1
	Aug	calendar month	3.253	0.270	< 0.001	2.9	1.9
	Jul		3.201	0.305	< 0.001	2.8	1.9
	Jun		3.116	0.341	< 0.001	2.5	2.0
	May		3.043	0.298	< 0.001	2.4	2.0
	Industrial NO_X emission site density (400 m)	sites/km^2	3.161	0.181	< 0.001	2.4	1.1
	Major roads (100 m)	km	4.591	0.694	< 0.001	1.9	1.7
	Apr		1.959	0.205	< 0.001	1.0	1.8
	Sep		1.893	0.199	< 0.001	1.0	1.9
	minor roads (300 m)	km	0.623	0.266	0.019	0.7	1.3
	Oct		1.358	0.130	< 0.001	0.5	1.9
	Major roads (500 m)	km	0.427	0.194	0.028	0.5	1.9
	Distance to coast	km	0.541	0.253	0.032	0.4	1.3
	Mar		1.100	0.100	< 0.001	0.3	1.8
	year	calendar year	−0.122	0.031	< 0.001	0.3	1.0
	Nov		0.630	0.094	< 0.001	0.1	1.8
	Jan		−0.161	0.070	0.022	0.0	1.8
	Feb		0.149	0.066	0.023	0.0	1.8

[a] Some variables were centred and standardised to make their parameter estimates more interpretable (see supplement);
[b] The unit decrease in model R^2 (%) when a variable is excluded. Variables that contribute more predictive ability lead to larger decreases when they are excluded.
[c] Percent RMS error is the overall average across the monitoring sites. Note: December was the reference month in the monthly models. All calendar month variables were significant at the 5% level except January in the monthly surface model. SE = standard error; VIF = variance inflation factor; RMS = root mean squared; ppb = parts per billion.

both vehicle and non-vehicle sources of NO_2, both of which contribute to ambient NO_2 and human exposure.

We found that satellite-derived NO_2 estimates from the Ozone Monitoring Instrument added the most predictive ability to 3 of our 4 models. Previous studies have reported pronounced reductions in model performance when satellite NO_2 is excluded (e.g. Novotny et al., 2011; Vienneau et al., 2013). Our findings further confirm the utility of satellite NO_2 in national-scale LUR, and the improvements in exposure assessment that it offers.

Notably, we found that the best annual and monthly models that included NO_2 tropospheric column observations exhibited slightly better predictive ability with comparable error to those that included estimates of surface NO_2 obtained by modelling surface-to-column ratios using WRF-Chem. This could reflect the fact that tropospheric columns are dominated by NO_2 in the part of the atmosphere closest to Earth's surface (i.e. the boundary layer), and are therefore useful proxies of relative ground-level concentrations (Richter et al., 2005). Also, the parameters selected in the process of modelling surface-to-column ratios (supplement, pages S4–S9) may add additional error into NO_2 estimates obtained using this method (Lamsal et al., 2008; Bechle et al., 2013). Modelling surface-to-column ratios is both computationally- and time-intensive and requires technical expertise. Our findings are promising for those who are interested in less complex approaches to NO_2 exposure assessment. We note, however, that these findings may be specific to the context of our study and are not necessarily applicable beyond that.

Our study has some important limitations. The monitoring data used to build the models came from only 68 sites, which is small when compared with other national LUR studies (e.g. Novotny et al., 2011; Vienneau et al., 2013), particularly when Australia's size is considered (supplement, Table S3; Johnson et al., 2010; Basagaña et al., 2012; Wang et al., 2012). Indeed, it was this paucity of monitoring that provided the initial motivation for our study. However, this means that model predictions may be valid only when applied to environments similar to those where monitoring was performed. We addressed this by comparing the summary statistics of predictors at the monitoring sites with those at the mesh block centroids that covered all of Australia (supplement, Table S11). We found no evidence to indicate that the monitoring sites on which the models were based differed markedly from the broader Australian context that they were

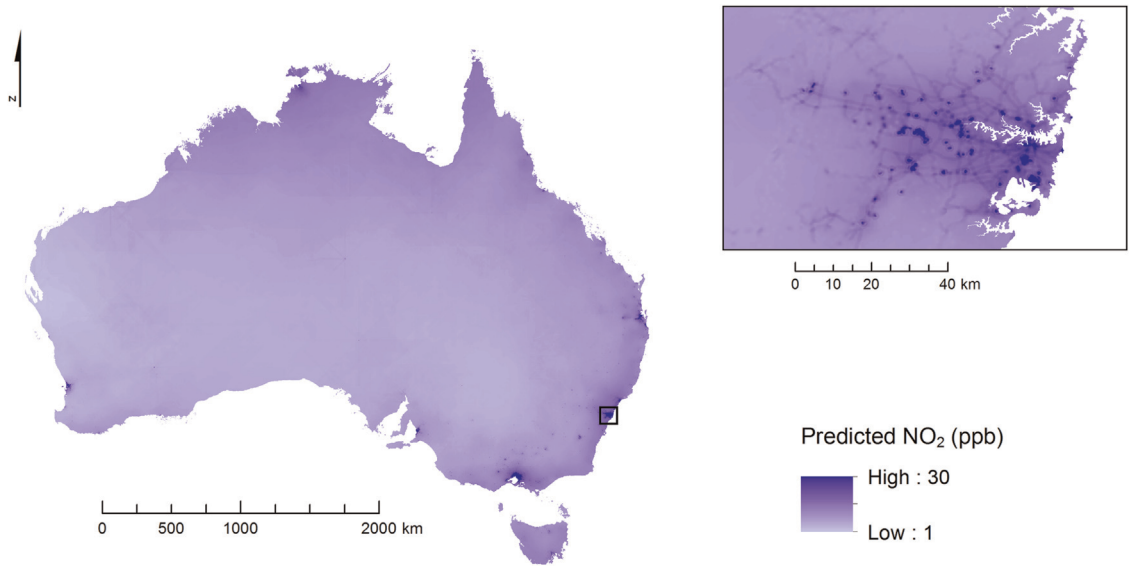

Fig. 1. Average NO_2 concentration in 2008 predicted at ~350,000 census mesh block centroids by the annual surface model. The inset focuses on the greater Sydney area, Australia's largest city (population ~4.5 million). The figure was produced by applying ordinary kriging to the mesh block predictions and is displayed at 100 m resolution.

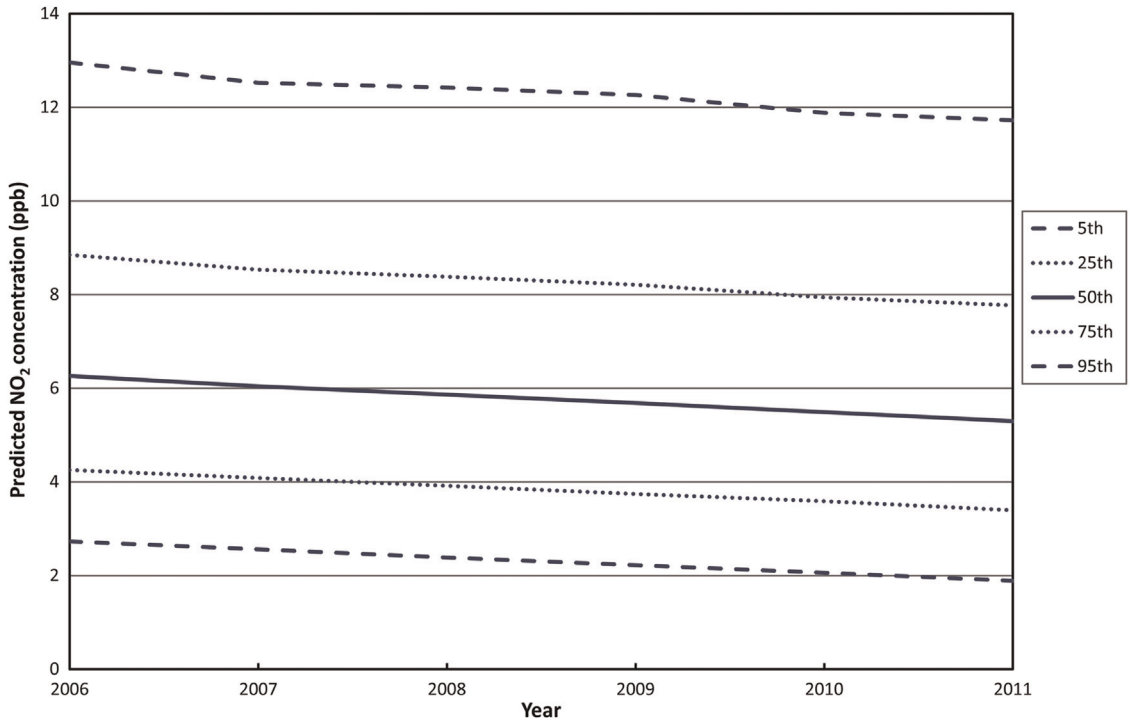

Fig. 2. Selected percentiles of annual average NO_2 predicted at ~350,000 census mesh block centroids by the annual surface model, 2006–2011.

applied to. However, the monitoring sites are primarily used for regulatory ambient air monitoring, and so they were not typically sited near substantial emission sources. For this reason, using our models to predict concentrations in pollution 'hot-spots' (such as road intersections or areas with very localised non-road emissions) should be undertaken with caution, and would require additional validation against measurements from the area of interest.

Because we used a generalised estimating equation we were unable to assess spatial autocorrelation in the model residuals. However, all other national satellite-based NO_2 models have reported that spatial autocorrelation was not present in model residuals, and this is also true of many non-satellite urban LUR models (Hoek et al., 2008; Hystad et al., 2011; Novotny et al., 2011; Vienneau et al., 2013). Also, our small data set prevented us from holding out some of the data for an independent evaluation (Hoek et al., 2008; Novotny et al., 2011; Wang et al., 2012), which has also been the case in other studies with limited monitoring data (e.g. Hystad et al., 2011). We instead used five-fold cross-validation to estimate our models' prediction error. We note that our R^2 values may be higher than would be observed with a new validation data set due to the relatively small number of monitoring sites and large number of predictors (Basagaña et al., 2012; Wang et al., 2012). Finally, we focussed on generating monthly and annual averages rather than daily estimates (e.g. Lee and Koutrakis, 2014). This enabled us to examine all of Australia, rather than a specific region or city.

Satellite-based LUR models hold promise for improving exposure assessment in epidemiological studies and have a diverse range of potential applications. They are particularly useful in locations with sparse or absent ground-based monitoring. Our models included both variables within different buffers (e.g. percent land use type, road length) and point variables (e.g. satellite NO_2, distance to coast). They permit unique predictions for a given set of input points (e.g. residential addresses). Our models are capable of capturing within-urban variability in concentrations, and although we did not aim to capture localised effects the models may also be able to capture some near-source (e.g. roads, industry) variability in certain areas (Hoek et al., 2008; Marshall et al., 2008). Because the models spanned the entire country there were no limitations around city-to-city transferability. Our models are the first that we are aware of to offer national coverage of Australia, and add to the growing international evidence regarding the utility of satellite-based LUR.

In summary, our satellite-based LUR models were able to capture ~80% of spatial variability in monthly and annual ambient NO_2 concentrations during 2006–2011 across Australia, a country with sparse ground-level monitoring. These models can be used to determine concentrations that individuals are exposed to at their residential address, or for larger spatial units (e.g. post code or suburb level) if their address is unknown due to confidentiality restrictions. They can also be used to refine and validate estimates of population-level exposures. With these applications in mind we are making our model predictions freely available to those who want to use them for research.

Acknowledgements

Please contact the corresponding author if you would like to use the model predictions described in the paper. LDK acknowledges an NHMRC Early Career (Australian Public Health) Fellowship (APP1036620). This material is partially based on work supported by the United States National Science Foundation under Grant No. 0853467. Computational resources and services used in this study were provided by the High Performance Computer and Research Support Unit, Queensland University of Technology, and the Research Computing Centre, The University of Queensland. Analyses and visualisations used in this study were produced with the Giovanni online data system, developed and maintained by the NASA GES DISC. We acknowledge the Aura mission for the production of the data used in this research effort, and the Netherlands Agency for Aerospace Programs in collaboration with the Finnish Meteorological Institute through their contribution to the Aura mission via the Ozone Monitoring Instrument. We thank the state and territory authorities in Australia that freely provided NO_2 monitoring data. We also acknowledge the free use of data provided by the Global Land Cover Facility, NOAA National Geophysical Data Centre, Australian Bureau of Meteorology, Australian Bureau of Statistics, and Australian National Pollutant Inventory. Roads and airports data were purchased from the Public Sector Mapping Agencies (Australia). Elevation data were purchased from Geoscience Australia.

Appendix A. Supplementary Information

Supplementary data associated with this article can be found in the online version at http://dx.doi.org/10.1016/j.envres.2014.09.011.

References

Alfons, A., 2012. cvTools: Cross-validation tools for regression models. R package version. Available online: ⟨http://CRAN.R-project.org/package=cvTools⟩ (accessed 10.06.14).

Australian Bureau of Statistics, 2011. Australian Statistical Geography Standard (ASGS): Volume 1 – Main Structure and Greater Capital City Statistical Areas, Australia. Available online: ⟨http://www.ausstats.abs.gov.au/ausstats/subscriber.nsf/0/D3DC26F35A8AF579CA257801000DCD7D/$File/1270055001_july%202011.pdf⟩ (accessed 10.06.14).

Australian Bureau of Statistics. Year Book Australia, 2012. Available online: ⟨http://www.ausstats.abs.gov.au/ausstats/subscriber.nsf/LookupAttach/1301.0Publication24.05.121/$file/13010_2012.pdf⟩ (accessed 10.06.14).

Australian Bureau of Statistics. Regional Population Growth, Australia, 2013a. Available online: ⟨http://www.abs.gov.au/ausstats/abs@.nsf/Products/3218.0~2012~Main+Features~Main+Features?OpenDocument⟩ (accessed 10.06.14).

Australian Bureau of Statistics. Australian Social Trends, April 2013b. Available online: ⟨http://www.abs.gov.au/AUSSTATS/abs@.nsf/Lookup/4102.0Main+Features30April+2013⟩ (accessed 10.06.14).

Australian Bureau of Statistics. Mesh Block Counts, 2013c. Available online: ⟨http://www.abs.gov.au/websitedbs/censushome.nsf/home/meshblockcounts⟩ (accessed 10.06.14).

Barnett, A.G., Williams, G.M., Schwartz, J., Neller, A.H., Best, T.L., Petroeschevsky, A. L., Simpson, R.W., 2005. Air pollution and child respiratory health: a case-crossover study in Australia and New Zealand. Am. J. Respir. Crit. Care Med. 171, 1272–1278.

Basagaña, X., Rivera, M., Aguilera, I., Agis, D., Bouso, L., Elosua, R., et al., 2012. Effect of the number of measurement sites on land use regression models in estimating local air pollution. Atmos. Environ. 54, 634–642.

Bechle, M.J., Millet, D.B., Marshall, J.D., 2013. Remote sensing of exposure to NO_2: satellite versus ground-based measurement in a large urban area. Atmos. Environ. 69, 345–353.

Beelen, R., Hoek, G., Fischer, P., van den Brandt, P.A., Brunekreef, B., 2007. Estimated long-term outdoor air pollution concentrations in a cohort study. Atmos. Environ. 41, 1343–1358.

Briggs, D.J., 2007. The use of GIS to evaluate traffic-related pollution. Occup. Environ. Med. 64, 1–2.

Briggs, D.J., Collins, S., Elliott, P., Fischer, P., Kingham, S., Lebret, E., et al., 1997. Mapping urban air pollution using GIS: a regression-based approach. Int. J. Geogr. Inf. Sci. 11, 699–718.

Friedman, J., Hastie, T., Tibshirani, R., 2010. Regularization paths for generalized linear models via coordinate descent. J. Stat. Softw. 33, 1–22.

Hart, J.E., Yanosky, J.D., Puett, R.C., Ryan, L., Dockery, D.W., Smith, T.J, et al., 2009. Spatial modeling of PM_{10} and NO_2 in the continential United States, 1985–2000. Environ. Health Perspect. 117, 1690–1696.

Hoek, G., Beelen, R., de Hoogh, K., Vienneau, D., Gulliver, J., Fischer, P., Briggs, D., 2008. A review of land-use regression models to assess spatial variation of outdoor air pollution. Atmos. Environ. 42, 7561–7578.

Hoffmann, B., Moebus, S., Möhlenkamp, S., Stang, A., Lehmann, N., Dragano, N., et al., 2007. Residential exposure to traffic is associated with coronary atherosclerosis. Circulation 116, 489–496.

Højsgaard, S., Halekoh, U., Yan, J., 2006. The R Package geepack for generalized estimating equations. J. Stat. Softw 15 (2), 1–11.

Hystad, P., Setton, E., Carvantes, A., Poplawski, K., Deschenes, S., Brauer, M., et al., 2011. Creating national air pollution models for population exposure assessment in Canada. Environ. Health Perspect. 119, 1123–1129.

Jerrett, M., Arain, A., Kanaroglou, P., Beckerman, B., Potoglou, D., Sahsuvaroglu, T., et al., 2005. A review and evaluation of intraurban air pollution exposure models. J. Expo Anal. Environ. Epidemiol. 15, 185–204.

Johnson, M., Isakov, V., Touma, J.S., Mukerjee, S., Özkaynak, H., 2010. Evaluation of land-use regression models used to predict air quality concentrations in an urban area. Atmos. Environ. 44, 3660–3668.

Lamsal, L.N., Martin, R.V., van Donkelaar, A., Steinbacher, M., Celarier, E.A., Bucsela, E., et al., 2008. Ground-level nitrogen dioxide concentrations inferred from the satellite-borne ozone monitoring instrument. J. Geophys. Res. 113, D16308.

Lamsal, L.N., Martin, R.V., van Donkelaar, A., Celarier, E.A., Bucsela, E.J., Boersma, K. F., et al., 2010. Indirect validation of tropospheric nitrogen dioxide the OMI satellite instrument: insight into the seasonal variation of nitrogen oxides at the northern midlatitudes. J. Geophys. Res. 115, D05302.

Lee, H.J., Koutrakis, P., 2014. Daily ambient NO_2 concentration predictions using satellite ozone monitoring instrument NO_2 data and land use regression. Environ. Sci. Technol 48, 2305–2311.

Levelt, P.F., Van den Oord, G.H.J., Dobber, M.R., Malkki, A., Huib, V., de Vries, J., Stammes, P., Lundell, J.O.V., Saari, H., 2006. The ozone monitoring instrument. IEEE Trans. Geosci. Remote Sens 44, 1093–1101.

Lim, S.S., Vos, T., Flaxman, A.D., Danaei, G., Shibuya, K., Adair-Rohani, H., et al., 2012. A comparative risk assessment of burden of disease and injury attributable to 67 risk factors and risk factor clusters in 21 regions, 1990–2010: a systematic analysis for the Global Burden of Disease Study 2010. Lancet 380, 2224–2260.

Marshall, J.D., Nethery, E., Brauer, M., 2008. Within-urban variability in ambient air pollution: comparison of estimation methods. Atmos.Environ. 42, 1359–1369.

Novotny, E.V., Bechle, M.J., Millet, D.B., Marshall, J.D., 2011. National satellite-based land-use regression: NO_2 in the United States. Environ. Sci. Technol 45, 4407–4414.

Richter, A., Burrows, J.P., Nusz, H., Granier, C., Niemeier, U., 2005. Increase in tropospheric nitrogen dioxide over China observed from space. Nature 437, 129–132.

Ritz, B., Yu, F., Fruin, S., Chapa, G., Shaw, G.M., Harris, J.A., 2002. Ambient air pollution and risk of birth defects in Southern California. Am. J. Epidemiol. 155, 17–25.

Rose, N., Cowie, C., Gillett, R., Marks, G.B., 2011. Validation of a spatiotemporal land use regression model incorporating fixed site monitors. Environ. Sci. Technol. 45, 294–299.

Su, J.G., Jerrett, M., Beckerman, B., 2009. A distance-decay variable selection strategy for land use regression modeling of ambient air pollution exposures. Sci. Tot. Environ. 407, 3890–3898.

Tibshirani, R., 1996. Regression shrinkage and selection via the Lasso. J. R. Stat. Soc. B 58, 267–288.

Vienneau, D., de Hoogh, K., Bechle, M.J., Beelen, R., van Donkelaar, A., Martin, R.V., et al., 2013. Western European land use regression incorporating satellite- and ground-based measurements of NO_2 and PM10. Environ. Sci. Technol. 47, 13555–13564.

Vienneau, D., de Hoogh, K., Beelen, R., Fischer, P., Hoek, G., Briggs, D., 2010. Comparison of land-use regression models between Great Britain and the Netherlands. Atmos. Environ. 44, 688–696.

Wang, M., Beelen, R., Eeftens, M., Meliefste, K., Hoek, G., Brunekreef, B., 2012. Systematic evaluation of land use regression models for NO_2. Environ. Sci. Technol. 46, 4481–4489.

SUPPLEMENTARY MATERIAL

A national satellite-based land-use regression model for air pollution exposure assessment in Australia

Luke D. Knibbs[1*]

Michael G. Hewson[2]

Matthew J. Bechle[3]

Julian D. Marshall[3]

Adrian G. Barnett[4]

[1] School of Population Health, The University of Queensland, Brisbane, Australia

[2] School of Geography, Planning and Environmental Management, The University of Queensland, Brisbane, Australia

[3] Department of Civil Engineering, The University of Minnesota, Minneapolis, USA

[4] School of Public Health and Social Work & Institute of Health and Biomedical Innovation, Queensland University of Technology, Brisbane, Australia

* Corresponding author
Public Health Building
The University of Queensland
Herston, QLD 4006, Australia
p: +61 7 3365 5409
e: l.knibbs@uq.edu.au

CONTENTS

1. METHODS

1.1 Satellite Retrieval of Nitrogen Dioxide

Background to the Ozone Monitoring Instrument

The Ozone Monitoring Instrument (OMI) observes atmospheric column density of NO_2 on a daily basis. It was launched in July 2004 and is one of the four instruments on board the NASA Earth Observing System Aura satellite designed to measure atmospheric trace gases and aerosol optical properties. The Aura satellite crosses the equator in a sun-synchronous polar orbit at approximately 13:30 hours local time for the daylight ascending orbit (Torres et al., 2007) and it passes over Australia in the mid- to late-afternoon. OMI measures top of atmosphere radiance from 270-500 nm in the ultraviolet and visible regions of the solar spectrum with a spatial resolution at nadir of 13 × 24 km (Levelt et al., 2006).

OMI NO_2 tropospheric column amount data (cloud screened at 30%) is available via the NASA Giovanni Aura/OMI online visualisation and analysis web site (http://gdata1.sci.gsfc.nasa.gov/daac-bin/G3/gui.cgi?instance_id=omi) (Acker & Leptoukh, 2007). The level 3 NO_2 concentration product, OMNO2d.003, is a daily, global dataset gridded at 0.25 × 0.25 degrees spatial resolution with units of 10^{15}molecules/cm^2. Briefly, the OMI-derived NO_2 algorithm: (1) takes radiance values in ultraviolet and visible bands known to absorb NO_2; (2) applies radiometric and de-striping corrections to column concentrations, and then; (3) calculates both tropospheric and stratospheric contributions to the atmospheric column NO_2 (for pixels which have less than 30% cloud cover) by incorporating satellite path slant corrections and a range of air mass factors, and; (4) converts the data from satellite swath grid to a consistent grid size (Bucsela et al., 2013). The NO_2 concentration at any given grid point is a weighted average of a number of OMI measurements, given the grid points are

calculated from OMI swath pixels which are 13 x 24 km at nadir but become larger toward the swath edge. The contribution of individual OMI pixels to NO_2 concentrations above a given geographic location is a function of the daily variance in Aura ephemeris.

While OMI tropospheric columns from the standard product are prone to seasonal bias (Lamsal et al., 2010), surface NO_2 estimates derived from OMI columns are well-correlated with corrected ground level measurements, with bias under 30% and without substantial seasonal variation (Lamsal et al., 2008; Lamsal et al., 2010; Novotny et al., 2011). Notwithstanding the confines of algorithms and a dynamic radiometric row anomaly more evident since January 2009, OMI NO_2 data sets offer consistent quality for quantitative investigations of the relationships between pollution, its sources, and populations (Lamsal et al., 2013).

1.2 Surface NO_2 estimates

Data source

We downloaded and subset the global daily average OMI tropospheric NO_2 data using NASA Giovanni website functions, for: (1) a spatial domain encompassing the Australian continent; and; (2) temporal aggregation to each calendar month from January 2006 through December 2011. The OMI row anomaly issue is normalised in the present study by the level 3 OMI NO_2 concentration product weighted average grid point calculation algorithm, as well as our selection of mean daily NO_2 concentration time averaged per month.

Modelling surface and tropospheric NO_2

We estimated the ground level NO_2 concentrations from the OMI observed tropospheric column NO_2 concentrations by determining surface-to-column ratios across Australia using

modelled ground-level and tropospheric NO_2 levels (Novotny et al., 2011). We used a gas phase chemistry and aerosol transport version of the Weather Research and Forecasting (WRF) model; WRF-Chem. WRF-Chem is a multi-scale, "on-line" fully connected, atmospheric chemistry edition of the WRF non-hydrostatic, fully compressible, community meteorological model (Grell et al., 2005). The fully coupled nature of the chemistry transport and meteorology applications means that during computation, the same transport schemes, horizontal and vertical grids, physics schemes and model time steps operate together, which removes the need for inter-model interpolation. Verification trials have shown that WRF-Chem improves on the previous coupled chemistry/meteorological models from which it was developed (Grell et al. 2005).

WRF-Chem requires the modeller to select combinations of computational schemes representing aerosol transport, gas-phase chemistry, atmospheric physics, cloud microphysics as well as land use energy-balance parameterisation. Furthermore, WRF-Chem configuration also involves making informed decisions on which meteorological boundary conditions, aerosol emissions (anthropogenic, biogenic and background), model domain sizes and grid spatial resolution to use. These model component choices are made considering any computational resource constraints.

In our study, 6 years of Australia-wide daily average NO_2 concentrations were required, ordinarily representing an extensive computational commitment. WRF-Chem version 3.5 was structured on The University of Queensland's Research Computing Centre (RCC) to produce the required output using 2 parallel batch runs of 64 CPUs each. With this constraint, WRF-Chem was configured using a single domain, 60 km spatial resolution, and time steps of 6 minutes to produce daily aggregated NO_2 concentrations. The WRF-Chem models contained

27 vertical levels. The WRF-Chem physics scheme configurations used in this study are listed in Table S1.

Table S1. WRF-Chem configuration.

Parameterisation	Selected Configuration Item
Microphysics scheme	Lin et al scheme
Cumulus scheme	Grell G3
Longwave radiation	RRTMG scheme
Shortwave radiation	RRTMG scheme
Planetary boundary layer	YSU scheme
Surface layer option	MM5 Monin-Obukhov scheme
Land surface option	Unified Noah land surface model
Chemistry driver	RADM2
Aerosol driver	MADE-SORGAM
Anthropogenic emissions	EDGAR 0.1 degree
Biogenic emissions	None
Background emissions	GOCART
Gas chemistry	On
Aerosol chemistry	On
Wet scavenging	Off
Vertical turbulent mixing	On
Cloud chemistry	Off

WRF-Chem meteorological boundary conditions were updated every six hours by data sourced from the National Centre for Environmental Prediction (NCEP) global 1-degree database of tropospheric analyses, which is a collection of meteorological observations used in the US Global Forecast System (GFS). Each model run calculated a month of NO_2 concentrations and included a model spin-up time of five days to ensure stable meteorological physics operation during the model run.

The WRF-Chem aerosol and gas phase molecule emissions were provided by two global data sets; GOCART global anthropogenic and background emissions as of 2006 with a spatial resolution of 1 degree (Chin et al., 2002), and the EDGAR (Emission Database for Global

Atmospheric Research) global anthropogenic emissions for 2005 with spatial resolution of 0.1 degree (Olivier et al., 2005).

WRF-Chem was configured with the MADE-SORGAM (Modal Aerosol Dynamics Model for Europe - Secondary Organic Aerosol Model) aerosol transport scheme and RADM2 (Regional Acid Deposition Model version 2) gas phase chemistry scheme because they offered timely model output. MADE was developed in Europe in 1998 (Ackermann et al., 1998), with the capacity to model secondary organic aerosol (SORGAM) added in 2001 as described by Schell et al. (2001). Fast et al. (2011) concluded that MADE-SORGAM performed as well as a more advanced 8-bin sectional aerosol parameterization while being computationally cheaper.

Since we used WRF-Chem to calculate an average daily ratio of surface-to-column NO_2 concentration aggregated to a monthly time scale Australia-wide, the model configuration trade-offs were considered suitable. In a study comparing a similarly configured WRF-Chem that measured anthropogenic emissions for the whole of Europe (albeit with a different anthropogenic emission source database), Tuccella et al. (2012) noted that WRF-Chem NO_2 replicated measured time-series NO_2 within ±15%.

The atmospheric chemistry model was used to create a ratio of near ground to tropospheric NO_2 concentrations for each month of the study. After each WRF-Chem run, NO_2 concentration at the 60 km spatial resolution was extracted and aggregated to the daily average for each calendar month of 2006 to 2011 using 'netCDF kitchen sink' LINUX file manipulation utilities. At each model grid-point the extraction created a netCDF file of latitude, longitude and NO_2 concentration in ppmv for each model level from near ground

level (i.e. surface) to the average height of the tropopause, which was set to 14 km and meant that the first 22 WRF-Chem model level NO_2 concentrations were extracted to represent the troposphere (i.e. column). The tropopause height varies latitudinally, seasonally and daily due to the heterogeneous nature of heat sources over time and space – according to figures presented by Sturman and Tapper (2006), a 14 km median tropopause height over Australia is reasonable. The NO_2 emission data sets were created in netCDF format because the intrinsic WRF-Chem model output file format can be read by ArcGIS (ESRI Inc., Redlands, USA), in which further OMI and model NO_2 comparison computation and emissions mapping was undertaken. The OMI tropospheric NO_2 data was sourced in text file format so that that ArcGIS point class shape-files could be readily produced for further processing.

Estimating surface NO_2 from OMI columns

We used ArcGIS to determine the ratio of WRF-Chem surface-to-column NO_2 at each grid point for each month of the study. We then applied this ratio to OMI tropospheric NO_2 columns to elicit a daily surface average NO_2 concentration at 0.25 x 0.25 degrees spatial resolution for each month from January 2006 to December 2011. Since the OMI and WRF-Chem NO_2 concentration had different spatial resolutions and therefore different grid structures, the ArcGIS model firstly calculated grid-point pairs using a GIS "one to one" spatial join and intersect procedure.

The maps of monthly and annually aggregated daily average OMI surface NO_2 concentrations were created using kriging interpolation in ArcGIS. Of the various techniques for treating trend common in atmospheric data geostatistical analysis, we chose universal kriging with linear drift, as described by Webster and Oliver (2007). Since universal kriging utilises localised parameter mean values a logarithmic transformation of the OMI and WRF-

Chem data sets was not warranted. This determination also acknowledges that the ArcGIS kriging semivariogram spatial correlation calculations using 12 points was only 0.04% of the grid points in the size of the domain – the data set mean has less influence and local clustering influences dominate the interpolation.

1.3 Land-use variables

Table S2. The type and source of independent land-use variables considered in the model.

Variable (units)	**Resolution**	**Point or buffer* estimate**	**Source** (all websites accessed on 02-Apr-2014)
OMI ground-level NO_2 (ppb) & OMI tropospheric NO2 column density (molecules × 10^{15} / cm^2)	13 × 24 km (nadir)	point	Aura OMI level-3 NO_2 product via NASA Giovani interface http://gdata1.sci.gsfc.nasa.gov/daac-bin/G3/gui.cgi?instance_id=omi Acker & Leptoukh (2007)
elevation (m)	30 m	point	Geoscience Australia 1-second smoothed digital elevation model derived from SRTM http://www.ga.gov.au/metadata-gateway/metadata/record/gcat_72759 Geoscience Australia (2011)
distance to coast (km)	-	point	Derived using 'Near' command in ArcGIS (excludes inland lakes)
annual & seasonal mean rainfall (mm)	2.5 km	point	Australian Bureau of Meteorology http://www.bom.gov.au/jsp/ncc/climate_averages/rainfall/index.jsp
annual & seasonal mean daily average temperature (°C)[a]	2.5 km	point	Australian Bureau of Meteorology http://www.bom.gov.au/jsp/ncc/climate_averages/temperature/index.jsp
annual & seasonal mean daily solar exposure (MJ/m^2)	5 km	point	Australian Bureau of Meteorology http://www.bom.gov.au/jsp/ncc/climate_averages/solar-exposure/index.jsp
tree cover (%)	250 m	buffer[i]	MODIS-derived vegetation continuous fields product for 2006 http://www.landcover.org/data/vcf/ DiMiceli et al. (2011)
impervious surfaces (%)	1 km	buffer[i]	NOAA constructed impervious surface area product 2000-2001 http://ngdc.noaa.gov/eog/dmsp/download_global_isa.html Elvidge et al. (2007)
major roads (km)[b]	-	buffer[j]	PSMA Australia Transport and Topography product** http://www.psma.com.au/?product=transport-topography PSMA (2013)
minor roads (km)[c]	-	buffer[j]	" "

total roads (= major roads + minor roads)	-	buffer[j]	" "
population density (persons/km^2)	mesh block[h]	buffer[i]	Australian Bureau of Statistics 2011 Census http://www.abs.gov.au/census
land use type (%)[d]	mesh block[h]	buffer[i]	" "
non-vehicle point source NO_X emissions (kg/yr)[e,f]	-	buffer[j]	Australia National Pollutant Inventory 2008/9 http://www.npi.gov.au/
airport (present/not present)[g]	-	buffer	PSMA Australia Transport and Topography product** http://www.psma.com.au/?product=transport-topography PSMA (2013)

NOTES:

[a] average daily minimum and maximum temperature were also included in the model
[b] major roads were defined as national/state highways, arterial roads (which are major connector roads for national and state highways) and sub-arterial roads (which are connectors between highways and/or arterial roads, or serve as an alternative for arterial roads) (PSMA, 2013)
[c] minor roads were defined as collector roads (which are connectors between sub-arterial roads, and distribute traffic to local roads) and local roads (which provide property access) (PSMA, 2013)
[d] four land use categories were examined – residential, commercial, industrial, and open space (which was the sum of water, parks and agricultural land [Rose et al., 2011])
[e] total (fugitive + non-fugitive) estimated NO_X emissions from the 1,857 industrial and commercial sites around Australia
[f] the average density (sites/km^2) of industrial and commercial sites emitting NO_X in each buffer was also included in the model
[g] there were few airports in the majority of buffers so they were defined as either 0 (not present) or 1 (present) (Hystad et al., 2011)
[h] a mesh block is the smallest spatial unit used in the Australian census and their size varies - on average they contain 62 people
[i] average of variable within buffer
[j] sum of variable within buffer

***** 22 circular buffers were created with radii of 100 m, 200 m, 300 m, 400 m, 500 m, 600 m, 700 m, 800 m, 1000 m, 1200 m, 1500 m, 1800 m, 2000 m, 2500 m, 3000 m, 3500 m, 4000 m, 5000 m, 6000 m, 7000 m, 8000 m, and 10,000 m (Novotny et al., 2011).

** Positional accuracy is ±2 m in urban areas, ±10 m in rural and remote areas. Attribute accuracy is 99.09% for key attributes (name and unique identifier) (PSMA, 2013).

1.4 Monitoring sites

Table S3. Location and number of monitoring sites in the 8 states and territories of Australia during the study period (2006-2011).

State/Territory	Population (2011)	Area (km^2)	*n* monitors	Monitor density (per 100,000 km^2)
Australian Capital Territory (ACT)	357,332	2,358	2	84
New South Wales (NSW)	6,916,971	800,809	20	2.5
Northern Territory (NT)	212,045	1,348,199	0	0
Queensland (QLD)	4,333,257	1,729,958	20	1.2
South Australia (SA)	1,596,615	984,179	5	0.5
Tasmania (TAS)	495,566	68,018	1	1.5
Victoria (VIC)	5,353,837	227,496	13	5.7
Western Australia (WA)	2,239,065	2,526,574	7	0.3
TOTAL	**21,504,688**	**7,687,591**	**68**	**0.9**

1.5 Model building

Variable processing

To improve model convergence and make the parameter estimates more interpretable, we centred and standardised some of the independent variables using the values shown below (Table S4). So, for example, the parameter estimates for elevation will be for a 100 metre increase, and the intercept of the model will be for an elevation of 20 metres.

Table S4. Values used to centre and standardise variables.

Variable	Centre	Standardise
Elevation (m)	20	100
Distance to coast (km)	10	50
Tree cover (%)	10	10
Impervious surface area (%)	10	10
Road lengths (km)*	Median	Inter-quartile range
Population density (persons/km^2)	500	1000
Land use (%)	10	10
Rainfall (mm)	100	100
Temperature (°C)	20	5
NPI NO_x*	Median	Inter-quartile range
Year	2008	1

* NPI NO_X refers to the total emissions (kg/yr) from point source sites within each buffer. The median and IQR were used for each buffer (from 100 m to 10,000 m).

Model validation

We used cross-validation rather than leave-one-out validation because some important predictors were only present at single sites, and hence the model failed to converge when these sites were removed. We examined the importance of these sites using the df-beta statistics.

We did not examine the spatial autocorrelation of the residuals because we used a generalised estimating equation (GEE) model (see discussion section of paper), which means that the

residuals include any remaining differences between monitors. This could have been avoided using a mixed model with a random station intercept, which would have given similar predictions and parameter estimates. However, we found that the GEE models had a better convergence and were easier to use in the cross-validation. Another advantage is that the GEEs give R^2 statistics that are based only on the predictors, whereas mixed models use the predictors and the random intercepts and hence would have given overly optimistic R^2 statistics for our models.

2. RESULTS

2.1 Measured NO_2 concentrations

Figures S1 and S2 present annual and monthly average NO2 concentrations measured at the monitoring sites, respectively.

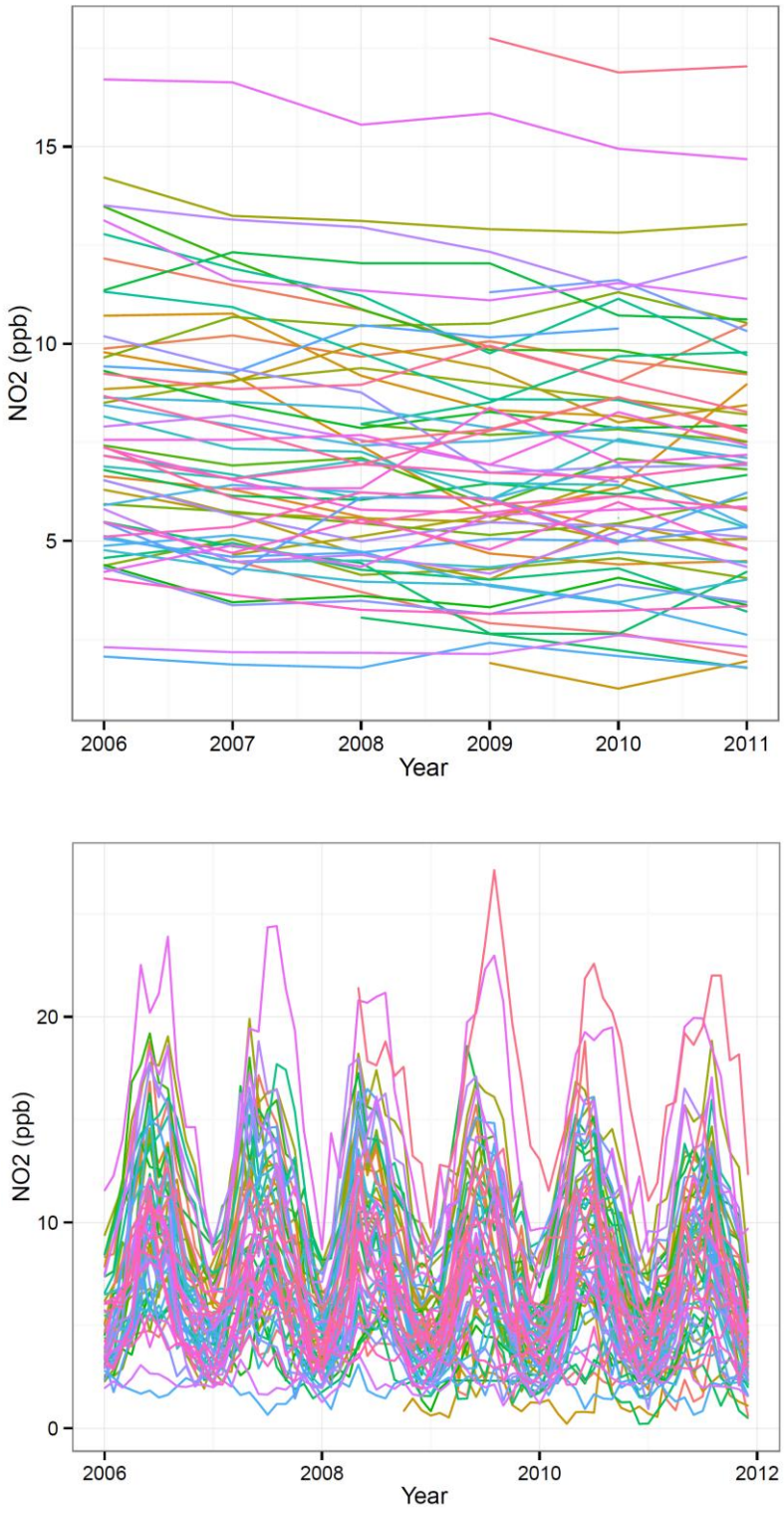

Figures S1 and S2. Time series of annual (top) monthly (bottom) NO_2 averages by monitoring site.

2.2 Results of variable selection process

Table S5 shows the results of the initial lasso variable selection process for the annual column model for the years 2006 to 2011 (1=Selected, 0=Not selected). Variables are ordered by selection frequency. Variables selected at least once are shown (26 variables), as only these were used in the second stage of variable selection (see methods section of main paper). Tables S6 shows the results of the lasso process for the annual surface model. Tables are not shown for the monthly models due to the large number of variables.

Table S5. Results of lasso variable selection for the annual column model.

	2006	2007	2008	2009	2010	2011	Total
Intercept	1	1	1	1	1	1	6
no2_column_mean	1	1	0	1	1	1	5
imp_sa_1200m...	0	1	1	1	0	1	4
min_rds10000m.km.	1	0	0	1	1	1	4
maj_rds800m.km.	0	0	0	1	1	1	3
NPI_sites_density500m.km2.	0	0	0	1	1	1	3
NPI_sites_density2000m.km2.	0	1	0	1	0	1	3
imp_sa_600m...	0	0	0	1	1	0	2
imp_sa_1500m...	1	1	0	0	0	0	2
imp_sa_1800m...	1	0	0	0	1	0	2
imp_sa_3500m...	0	0	1	1	0	0	2
NPI_sites_density10000m.km2.	0	0	0	1	1	0	2
imp_sa_500m...	0	0	0	0	1	0	1
imp_sa_1000m...	0	0	0	0	0	1	1
maj_rds500m.km.	0	0	0	0	1	0	1
maj_rds3500m.km.	0	1	0	0	0	0	1
min_rds8000m.km.	1	0	0	0	0	0	1
tot_rds8000m.km.	0	1	0	0	0	0	1
tot_rds10000m.km.	0	1	0	0	0	0	1
industrial10000m...	0	0	0	0	1	0	1
openspace10000m...	0	0	0	0	1	0	1
NPI_sites_density400m.km2.	0	0	0	0	1	0	1
NPI_sites_NOx_total500m.kg.	0	1	0	0	0	0	1
NPI_sites_density1000m.km2.	0	0	0	0	1	0	1
NPI_sites_density3000m.km2.	0	0	0	0	1	0	1
NPI_sites_density7000m.km2.	0	0	0	1	0	0	1

Table S6. Results of lasso variable selection for the annual surface model.

	2006	2007	2008	2009	2010	2011	Total
Intercept	1	1	1	1	1	1	6
imp_sa_1200m...	0	1	1	1	0	1	4
min_rds10000m.km.	1	0	0	1	1	1	4
imp_sa_1800m...	1	1	0	0	1	0	3
NPI_sites_density500m.km2.	0	0	0	1	1	1	3
NPI_sites_density2000m.km2.	0	1	0	1	1	0	3
no2_surface_mean	1	1	0	0	1	0	3
imp_sa_600m...	0	0	0	1	1	0	2
imp_sa_1500m...	1	1	0	0	0	0	2
imp_sa_3500m...	0	0	1	1	0	0	2
maj_rds800m.km.	0	0	0	1	1	0	2
NPI_sites_NOx_total500m.kg.	1	1	0	0	0	0	2
NPI_sites_density10000m.km2.	0	0	0	1	1	0	2
imp_sa_500m...	0	0	0	0	1	0	1
imp_sa_1000m...	0	0	0	0	0	1	1
maj_rds3500m.km.	0	1	0	0	0	0	1
maj_rds5000m.km.	0	1	0	0	0	0	1
tot_rds10000m.km.	0	1	0	0	0	0	1
pop_dens5000m.km2.	1	0	0	0	0	0	1
industrial10000m...	0	0	0	0	1	0	1
openspace10000m...	0	0	0	0	1	0	1
NPI_sites_density400m.km2.	0	0	0	0	1	0	1
NPI_sites_NOx_total400m.kg.	0	0	0	0	1	0	1
NPI_sites_density1000m.km2.	0	0	0	0	1	0	1
NPI_sites_density3000m.km2.	0	0	0	0	1	0	1

2.3 Model checking

Figures S3, S4, S5, and S6 show model residuals and Cook's distance for the annual column model, annual surface model, monthly column model and monthly surface model, respectively.

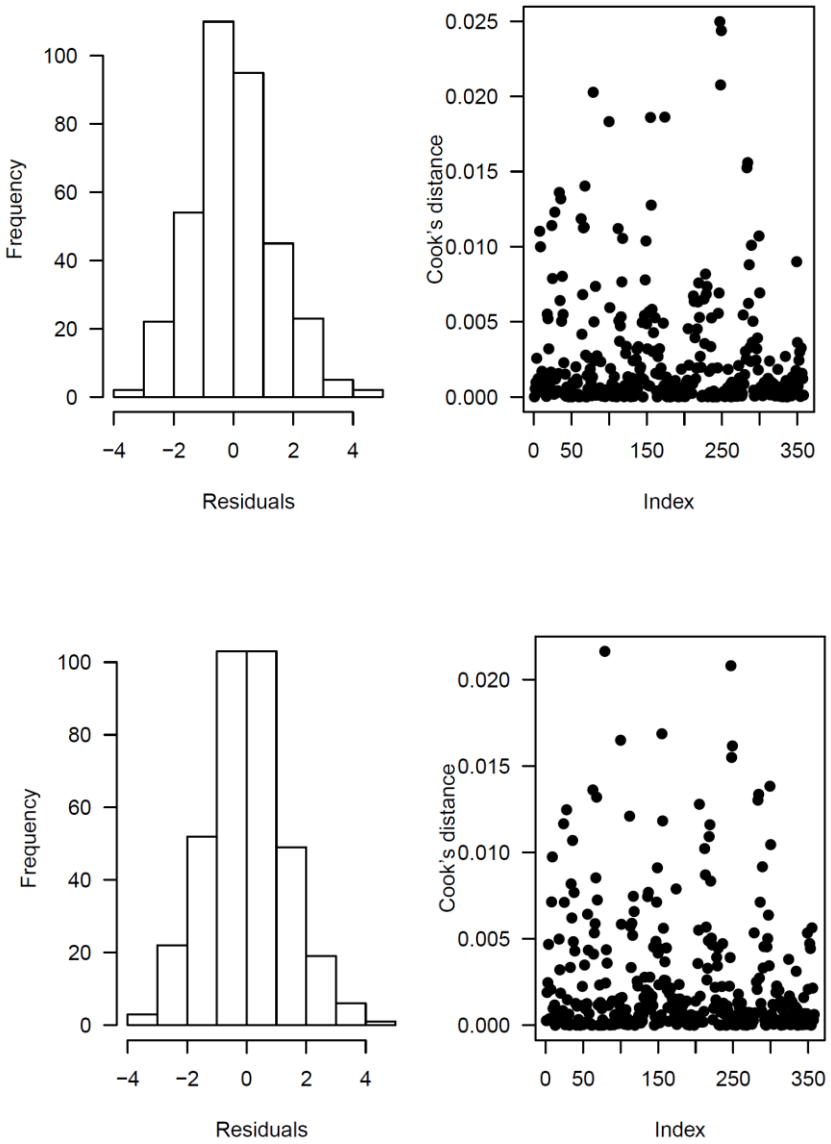

Figure S3 and S4. Model residuals and Cook's distance for annual column (top) and surface (bottom) models.

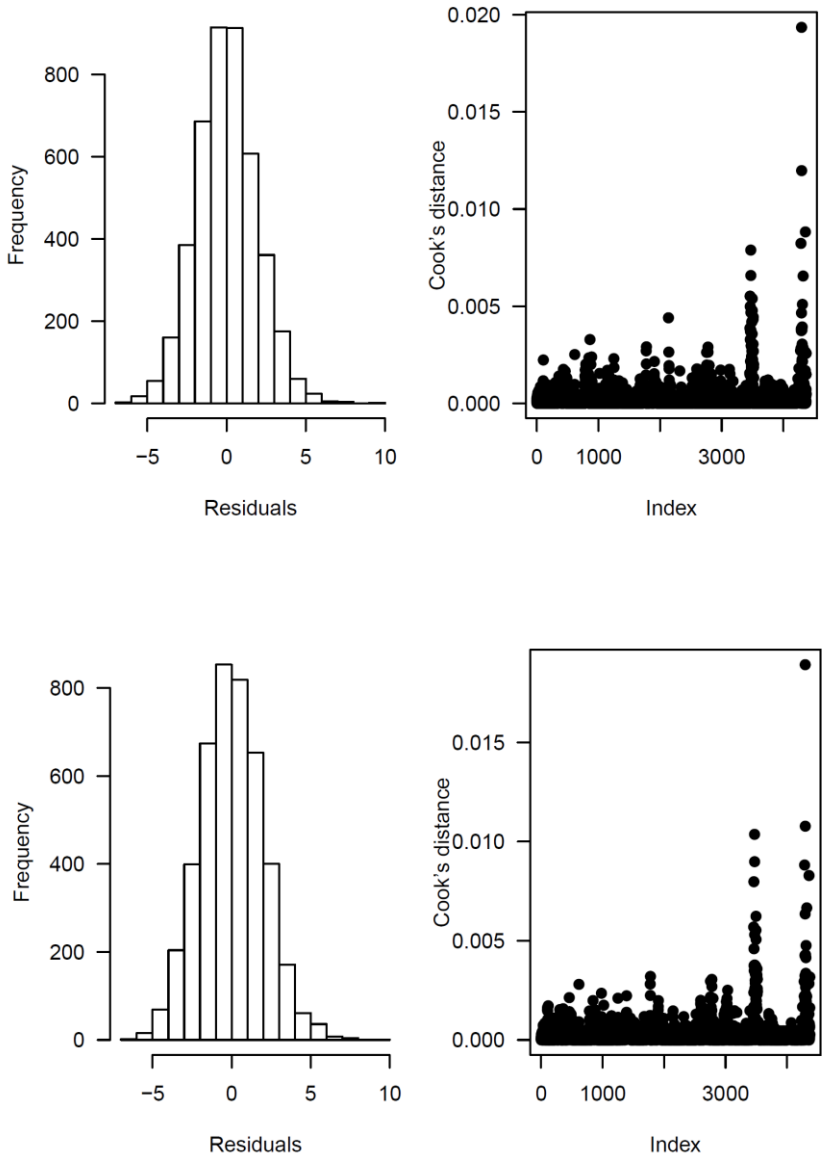

Figure S5 and S6. Model residuals and Cook's distance for monthly column (top) and surface (bottom) models.

We selected the NO_2 monitoring station with the highest Cook's distance from each model and compared it against three randomly chosen comparisons. Tables S7, S8, S9 and S10 show the results for the annual column, annual surface, monthly column and monthly surface models, respectively. We used this information to examine influential monitoring sites and check that their influence had a plausible basis. All of the largest Cook's distances were well below the commonly used threshold of 1.

Table S7. Dependent and standardised independent variables for the monitoring station with highest Cook's distances in the annual column model (Randwick) and three randomly chosen comparisons.

site_name	Randwick	Caversham	Wynnum	Bringelly
no2.mean.mean	6.728830	5.765494	7.825467	6.295198
imp_sa_1200m...	4.24	-0.21	0.27	-0.91
no2_column_mean	2.73	1.14	1.79	3.05
maj_rds500m.km.	-0.65	0.05	-0.65	-0.65
openspace10000m...	1.17	4.23	1.42	4.97
NPI_sites_density400m.km2.	0	0	0	0
NPI_sites_density1000m.km2.	0.0	0.0	0.3	0.0
industrial10000m...	-0.05	-0.31	2.75	-0.99
year.c	1	3	1	-2

Table S8. Dependent and standardised independent variables for the monitoring station with highest Cook's distances in the annual surface model (Dandenong) and three randomly chosen comparisons.

site_name	Dandenong	Kensington	Mountain_Creek	Traralgon
no2.mean.mean	9.649455	4.015835	4.453548	6.602205
imp_sa_1200m...	1.75	0.53	0.00	0.10
no2_surface_mean	1.38	0.35	0.18	0.48
maj_rds500m.km.	1.35	0.55	0.25	0.15
openspace10000m...	2.71	3.50	3.64	7.52
summer_mean_daily_solar.mJm.2.	23	26	23	22
NPI_sites_density400m.km2.	0	0	0	0
year.c	-2	1	3	2
industrial10000m...	0.26	-0.77	-0.81	-0.72
NPI_sites_density1000m.km2.	0.3	0.0	0.0	0.0

Table S9. Dependent and standardised independent variables for the monitoring station with highest Cook's distances in the monthly column model (Woolloongabba) and three randomly chosen comparisons.

site_name	Woolloongabba	Pinkenba	Liverpool	Duncraig
no2.mean.mean	27.123295	10.498651	9.772943	13.818460
Jan	0	0	0	0
Feb	0	0	0	0
Mar	0	0	0	0
Apr	0	1	0	0
May	0	0	0	0
Jun	0	0	0	1
Jul	0	0	0	0
Aug	1	0	0	0
Sep	0	0	0	0
Oct	0	0	1	0
Nov	0	0	0	0
min_rds8000m.km.	1.08432755	0.05189805	0.74257050	0.73486985
no2_column_mean	2.4	1.7	2.3	1.5
maj_rds100m.km.	0.4	0.0	0.0	0.0
NPI_sites_density400m.km2.	2	0	0	0
min_rds300m.km.	-0.35	-0.25	0.20	0.65
maj_rds500m.km.	1.95	-0.15	-0.15	0.35
dist_coast_noriver.km.	0.058	-0.172	0.238	-0.132
industrial10000m...	0.00	2.36	-0.15	-0.40
year.c	1	1	1	-2

Table S10. Dependent and standardised independent variables for the monitoring station with highest Cook's distances in the monthly surface model (Woolloongabba) and three randomly chosen comparisons.

site_name	Woolloongabba	Kembla_Grange	Elizabeth_Downs	Kensington
no2.mean.mean	27.123295	5.906775	4.963476	3.992169
Jan	0	0	0	0
Feb	0	0	0	0
Mar	0	0	0	0
Apr	0	0	0	0
May	0	0	0	0
Jun	0	0	0	0
Jul	0	0	0	0
Aug	1	1	0	0
Sep	0	0	0	0
Oct	0	0	1	1
Nov	0	0	0	0
imp_sa_500m...	3.50	-0.60	0.55	0.50
no2_surface_mean	0.6	0.7	0.3	0.3
NPI_sites_density1000m.km2.	0.3	0.0	0.0	0.0
min_rds8000m.km.	1.08432755	-0.17608460	0.04083514	0.72933839
NPI_sites_density400m.km2.	2	0	0	0
industrial10000m...	0.00	-0.28	-0.79	-0.77
maj_rds100m.km.	0.4	0.0	0.0	0.0
year.c	1	-2	-2	-1

Figures S7, S8, S9, and S10 show boxplots of df-beta statistics for the annual column model, annual surface model, monthly column model and monthly surface model, respectively. These highlight influential monitoring stations for each variable in the models. These were used in combination with the Cook's distance data presented above to identify and investigate influential observations. These were then checked for correctness (i.e. no errors in input data) and plausibility (i.e. a real-world basis for their influence [such as proximity to a high emitting industrial NO_X source]). Generally, the most influential variable was the industrial site density. These variables were positively skewed with many zero values and occasional high values, which increases the chances of them being influential. Industrial sites are a plausible source of NO_2 and none of the changes in the parameter slopes in the df-beta plots were extreme or counter-intuitive.

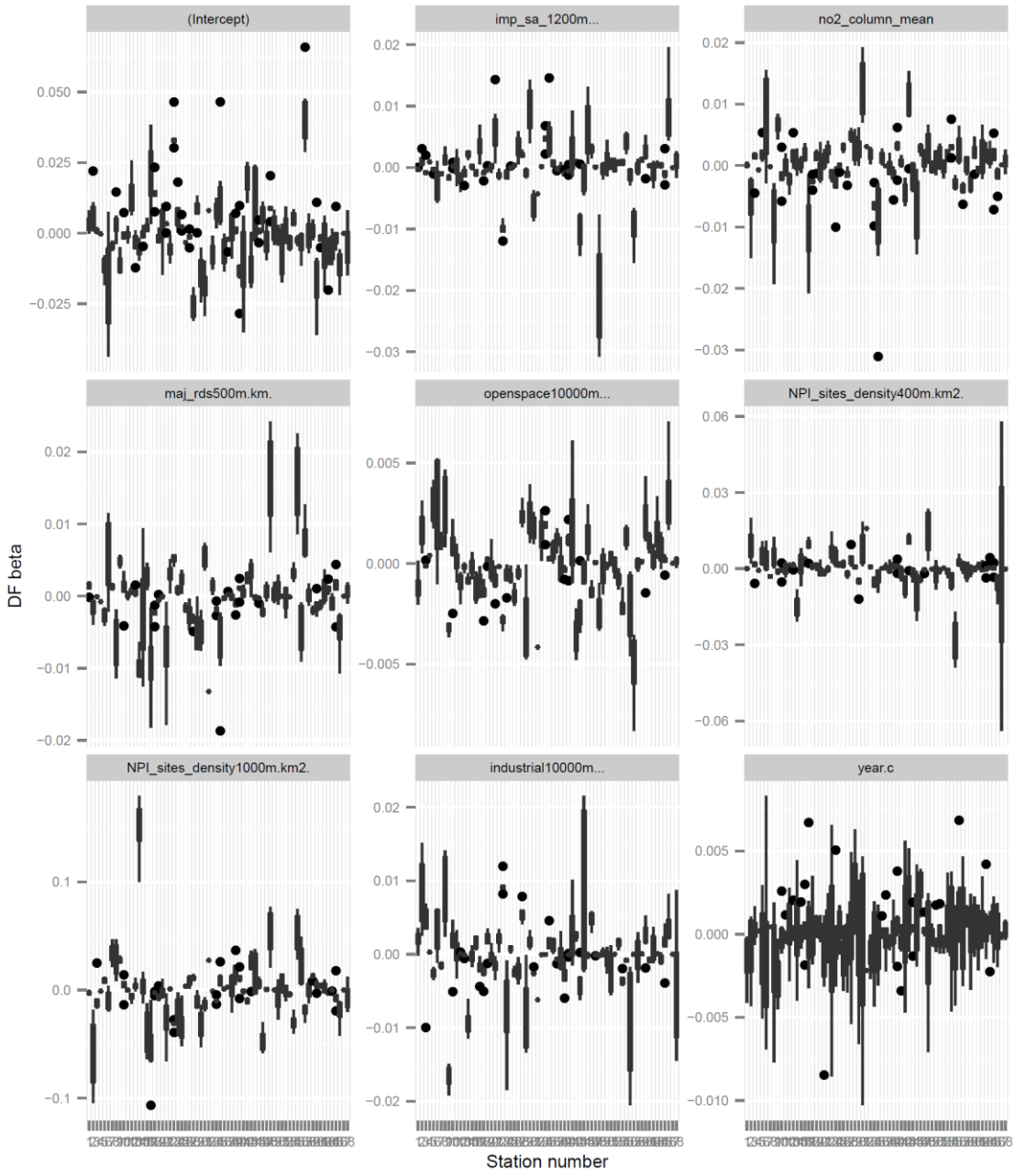

Figure S7. Boxplot of df-beta statistics for each variable in the annual column model.

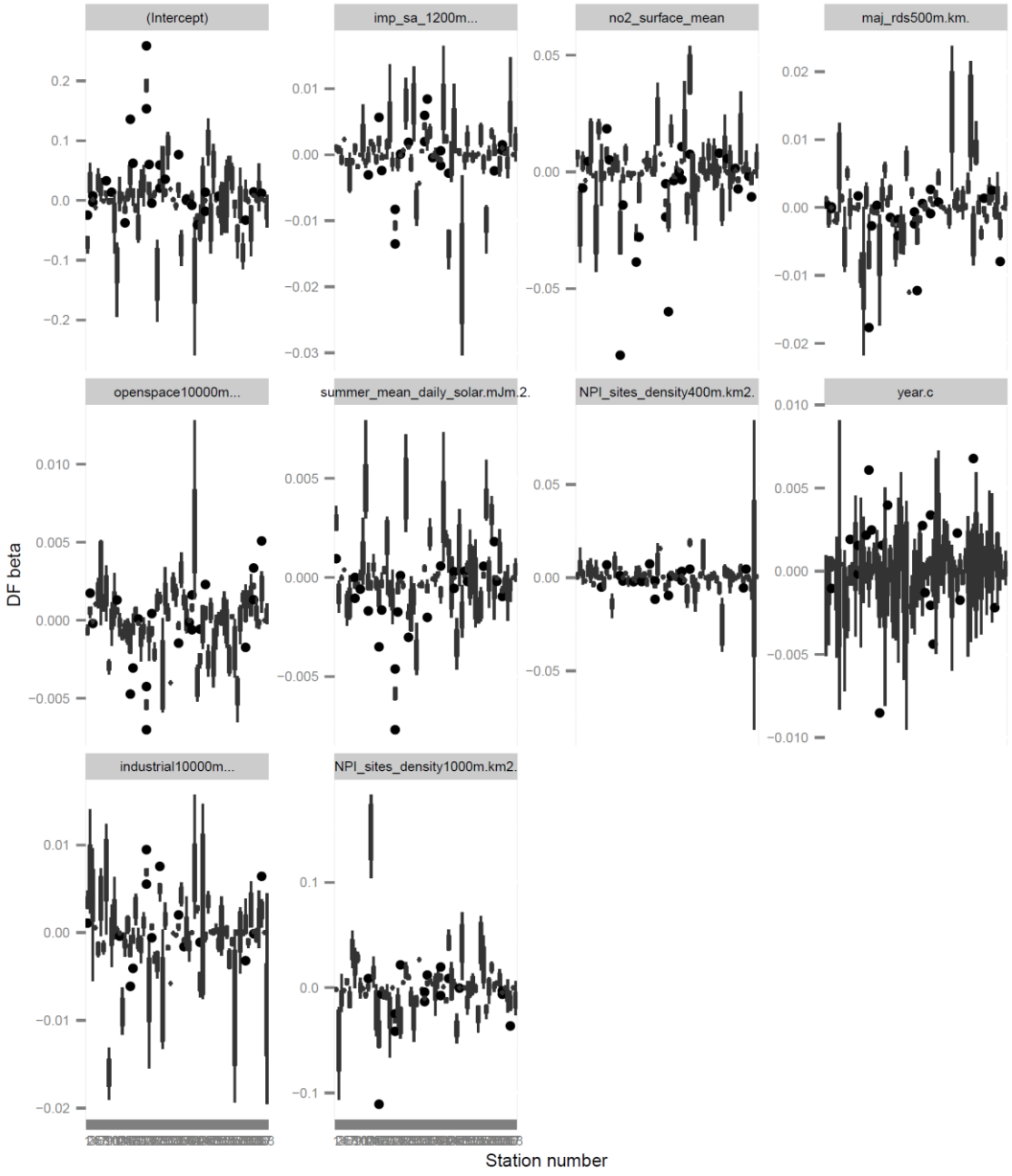

Figure S8. Boxplot of df-beta statistics for each variable in the annual surface model.

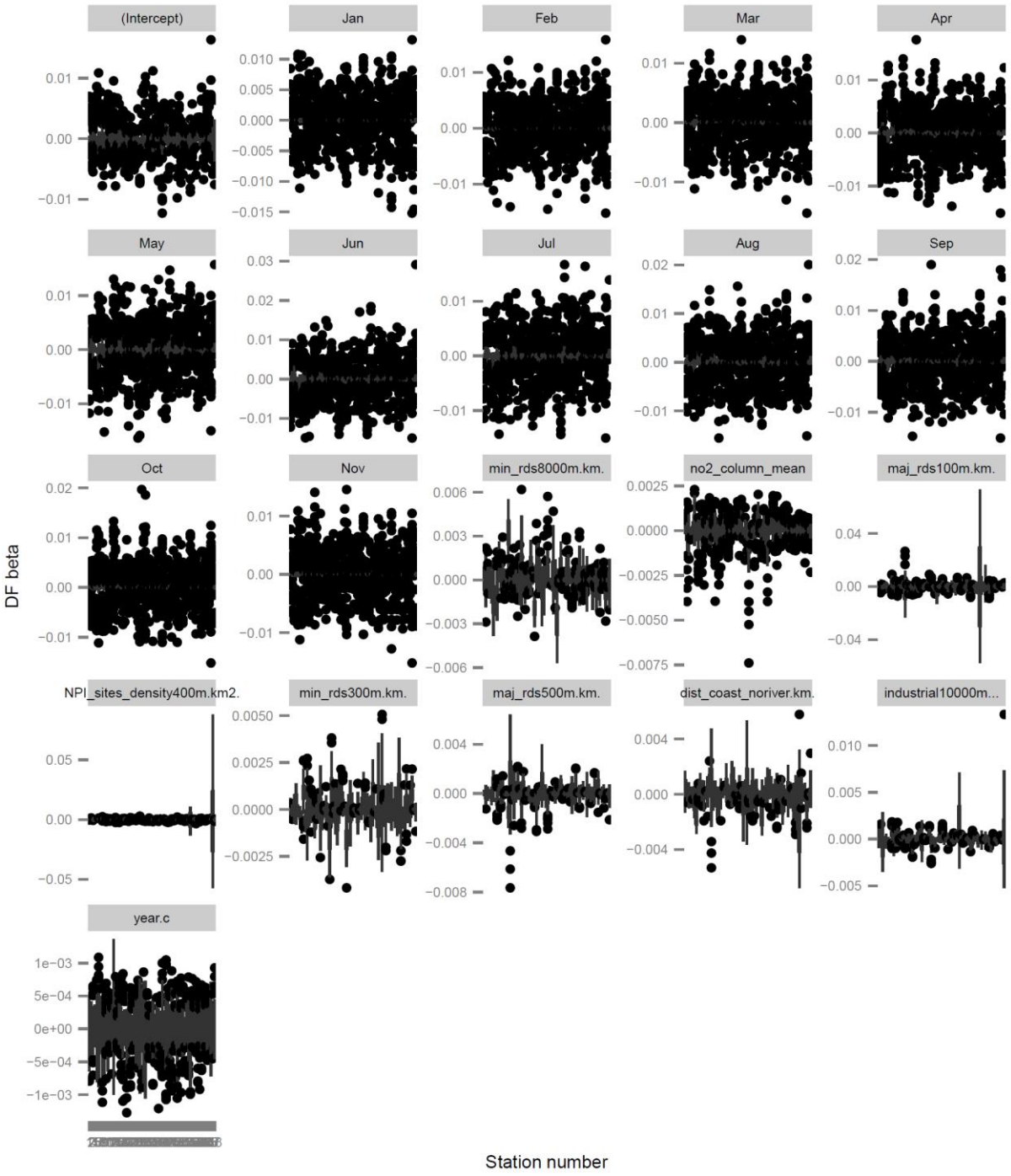

Figure S9. Boxplot of df-beta statistics for each variable in the monthly column model.

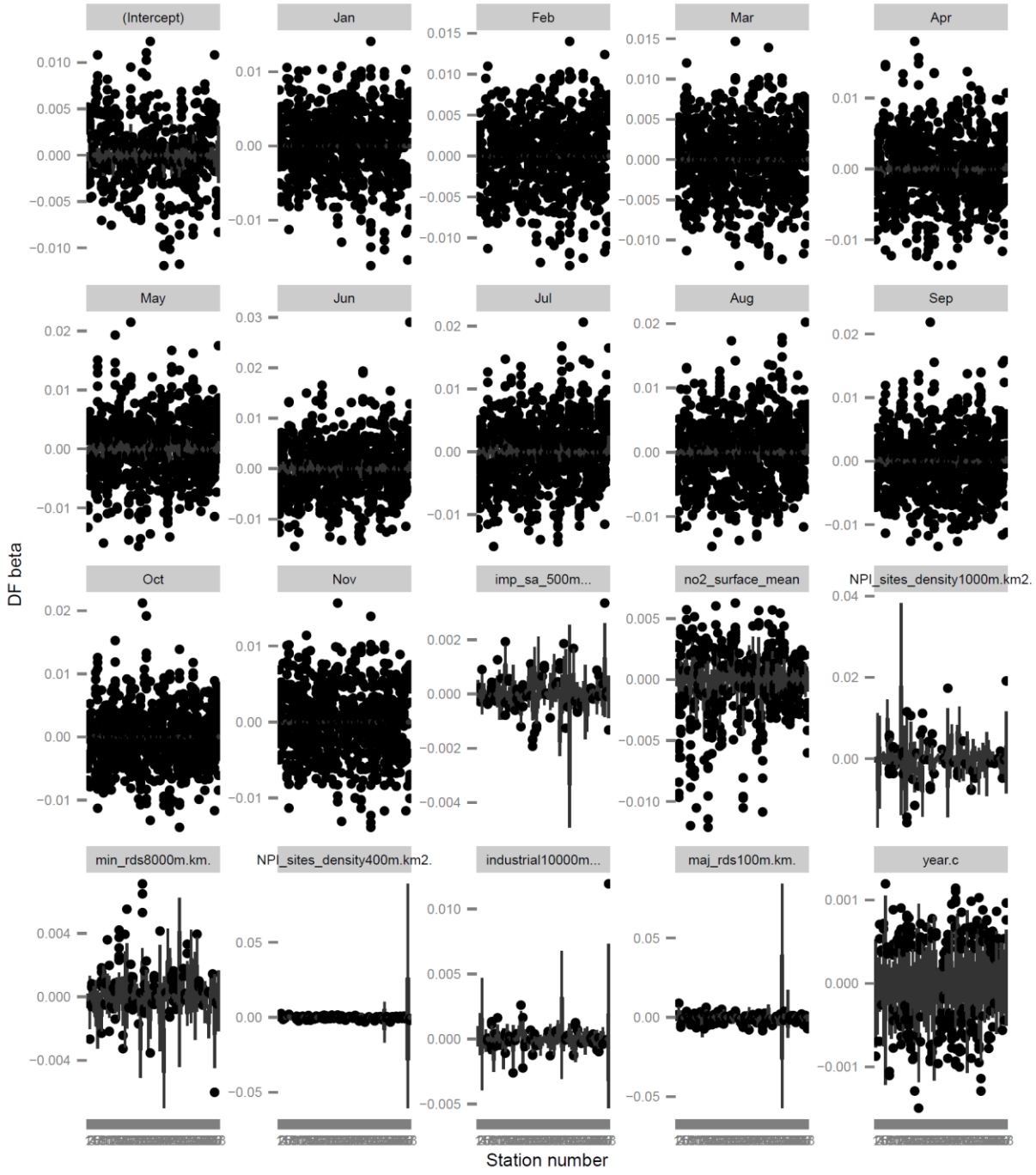

Figure S10. Boxplot of df-beta statistics for each variable in the monthly surface model.

2.4 Selected percentiles of predictors

For the models to be applicable to areas beyond just those where the NO_2 monitors were located, it is important that the predictors span a sufficient range and one that is representative of the areas that they will be applied to (Novotny et al., 2011). We compared the summary statistics for the predictors at the 68 monitoring sites used to build the models (which included a variety of different land use settings) to the summary statistics of predictors in the annual (surface and column) models at the ~350,000 census mesh block centroids spread across the entirety of Australia. Table S11 summarises the results. The statistics were very similar and suggests no evidence that monitoring sites differed markedly from the broader Australian context. We did not compare the statistics for the monthly models due to the large number of results (144). However, the main predictors in the monthly models are similar to those in the annual models (e.g. major and minor roads, impervious surfaces, industrial land use, industrial site density), and all of which are closely matched to the distributions observed around the country. This gives us no reason to suspect issues around representativeness for either of the monthly models.

2.5 Comparison of surface and column model predictions

Table S12 presents the summary statistics for NO_2 concentrations predicted at the ~350,000 mesh block centroids by the annual surface and column models. The table highlights that the predictions were almost identical. Population-weighted and unweighted mean concentrations are also shown. Table S13 presents the summary statistics for concentrations predicted by the two models at the ~57,000 mesh block centroids that make up the greater Sydney area, which is Australia's most populous city (4.4 million).

Table S11. Selected percentiles for predictors (annual surface and column models) at the monitoring sites and mesh block centroids.

	Monitoring sites (*n* = 68)					Mesh blocks (*n* = 344,500)				
Predictor	**5th**	**25th**	**50th**	**75th**	**95th**	**5th**	**25th**	**50th**	**75th**	**95th**
impervious surfaces 1200 m (%)	0.0	7.5	15.0	26.5	45.0	0.0	1.8	10.0	23.3	47.9
major roads 500 m (km)	0.0	0.0	0.6	1.0	2.4	0.0	0.0	0.7	1.1	2.3
summer mean daily solar radiation (MJ/m^2)	21.0	22.0	23.0	24.0	28.0	21.0	22.0	23.0	25.0	28.0
open space 10,000 m (%)	16.3	25.6	51.2	72.0	96.2	16.0	30.7	59.7	89.4	99.8
industrial NO_X emission site density 400 m ($sites/km^2$)	0.0	0.0	0.0	0.0	0.0	0.0	0.0	0.0	0.0	0.0
industrial NO_X emission site density 1,000 m ($sites/km^2$)	0.0	0.0	0.0	0.0	0.3	0.0	0.0	0.0	0.0	0.3
industrial land use 10,000 m (%)	0.0	2.3	6.1	9.9	22.8	0.0	0.3	2.6	6.9	13.1
OMI NO_2 surface mean 2006 (ppb)	0.1	0.3	0.4	0.9	1.4	0.1	0.2	0.4	1.0	1.4
OMI NO_2 surface mean 2007 (ppb)	0.2	0.3	0.4	0.9	1.1	0.1	0.2	0.4	0.9	1.2
OMI NO_2 surface mean 2008 (ppb)	0.2	0.3	0.4	0.8	1.2	0.1	0.2	0.3	0.9	1.3
OMI NO_2 surface mean 2009 (ppb)	0.2	0.3	0.4	0.8	1.3	0.1	0.2	0.4	0.8	1.3
OMI NO_2 surface mean 2010 (ppb)	0.1	0.3	0.4	0.7	1.2	0.1	0.2	0.4	0.8	1.2
OMI NO_2 surface mean 2011 (ppb)	0.1	0.3	0.4	0.8	1.1	0.1	0.2	0.3	0.8	1.1
OMI NO_2 column mean 2006 ($molecules \times 10^{15}/cm^2$)	1.0	1.3	2.0	3.2	4.0	0.7	1.0	1.5	3.3	4.0
OMI NO_2 column mean 2007 ($molecules \times 10^{15}/cm^2$)	1.0	1.3	2.0	3.0	3.7	0.7	1.0	1.5	3.2	3.7
OMI NO_2 column mean 2008 ($molecules \times 10^{15}/cm^2$)	1.0	1.3	1.7	3.0	3.3	0.7	1.0	1.4	3.0	3.3
OMI NO_2 column mean 2009 ($molecules \times 10^{15}/cm^2$)	1.1	1.3	1.8	2.7	4.0	0.7	1.0	1.4	2.7	4.0
OMI NO_2 column mean 2010 ($molecules \times 10^{15}/cm^2$)	1.0	1.2	1.7	2.7	3.4	0.7	1.0	1.3	2.7	3.4
OMI NO_2 column mean 2011 ($molecules \times 10^{15}/cm^2$)	1.0	1.2	1.7	2.8	3.4	0.7	1.0	1.4	2.9	3.4

Table S12. Summary statistics for NO_2 concentrations predicted at each mesh block centroid across Australia by the annual surface and column models.

	Surface model						Column model					
Predicted NO_2 (ppb)	**2006**	**2007**	**2008**	**2009**	**2010**	**2011**	**2006**	**2007**	**2008**	**2009**	**2010**	**2011**
Min.	1.2	1.1	0.9	0.7	0.6	0.4	2.0	1.8	1.7	1.6	1.4	1.3
1st	2.1	1.9	1.7	1.6	1.4	1.2	2.5	2.3	2.2	2.0	1.8	1.8
5th	2.7	2.6	2.4	2.2	2.1	1.9	2.7	2.5	2.4	2.2	2.1	2.0
25th	4.3	4.1	3.9	3.7	3.6	3.4	4.1	3.9	3.7	3.6	3.4	3.3
50th	6.3	6.0	5.9	5.7	5.5	5.3	6.2	6.0	5.8	5.7	5.4	5.3
75th	8.9	8.5	8.4	8.2	7.9	7.8	8.9	8.6	8.2	8.1	7.8	7.8
95th	13.0	12.5	12.4	12.3	11.9	11.7	13.1	12.7	12.2	12.4	11.9	11.8
99th	16.9	16.5	16.4	16.2	15.8	15.7	17.2	16.8	16.3	16.4	15.9	15.9
Max.	38.3	38.1	37.9	37.7	37.5	37.4	38.2	38.0	37.6	37.6	37.3	37.1
Unweighted mean	6.9	6.6	6.5	6.3	6.1	5.9	6.8	6.6	6.3	6.3	6.0	5.9
Population-weighted mean	7.3	7.0	6.9	6.7	6.5	6.3	7.3	7.1	6.7	6.7	6.4	6.3

Table S13. Summary statistics for NO_2 concentrations predicted at each mesh block centroid in the greater Sydney area by the annual surface and column models.

	Surface model						Column model					
Predicted NO_2 (ppb)	**2006**	**2007**	**2008**	**2009**	**2010**	**2011**	**2006**	**2007**	**2008**	**2009**	**2010**	**2011**
Min.	4.1	3.9	3.7	3.5	3.4	3.2	3.2	3.1	2.9	2.8	2.7	2.5
1st	5.3	5.0	4.7	4.5	4.3	4.1	4.9	4.6	4.4	4.0	3.9	3.9
5th	6.1	5.8	5.6	5.4	5.1	5.0	6.1	5.7	5.5	5.0	4.9	4.9
25th	7.9	7.6	7.3	7.1	6.8	6.7	7.9	7.6	7.2	6.7	6.6	6.7
50th	9.8	9.5	9.2	9.0	8.7	8.6	9.8	9.4	9.0	8.4	8.4	8.4
75th	11.5	11.2	11.0	10.7	10.4	10.3	11.6	11.2	10.8	10.3	10.2	10.3
95th	14.7	14.5	14.2	13.9	13.6	13.6	15.0	14.7	14.3	13.7	13.6	13.7
99th	18.2	18.0	17.7	17.4	17.1	17.1	18.5	18.1	17.7	17.2	17.0	17.1
Max.	37.4	37.2	36.9	36.6	36.3	36.3	38.0	37.9	37.5	36.9	36.7	36.9
Unweighted mean	9.9	9.7	9.4	9.1	8.9	8.8	10.0	9.6	9.3	8.8	8.7	8.7
Population-weighted mean	9.9	9.6	9.3	9.1	8.8	8.7	9.9	9.6	9.2	8.7	8.6	8.7

REFERENCES

Acker, J.G.; Leptoukh, G. Online Analysis Enhances Use of NASA Earth Science Data. Eos, Trans AGU. 88:14-17; 2007

Ackermann, I.J.; Hass, H.; Memmesheimer, M.; Ebel, A.; Binkowski, F.S.; Shankar, U. Modal aerosol dynamics model for Europe: development and first applications. Atmospheric Environment. 32:2981-2999; 1998

Bucsela, E.J.; Krotkov, N.A.; Celarier, E.A.; Lamsal, L.N.; Swartz, W.H.; Bhartia, P.K.; Boersma, K.F.; Veefkind, J.P.; Gleason, J.F.; Pickering, K.E. A new stratospheric and tropospheric NO2 retrieval algorithm for nadir-viewing satellite instruments: applications to OMI. Atmos Meas Tech. 6:2607-2626; 2013

Chin, M.; Ginoux, P.; Kinne, S.; Torres, O.; Holben, B.N.; Duncan, B.N.; Martin, R.V.; Logan, J.A.; Higurashi, A.; Nakajima, T. Tropospheric Aerosol Optical Thickness from the GOCART Model and Comparisons with Satellite and Sun Photometer Measurements. Journal of the Atmospheric Sciences. 59:461-483; 2002

DiMiceli, C.M.; Carroll, M.L.; Sohlberg, R.A.; Huang, C.; Hansen, M.C.; Townshend , J.R.G. Annual Global Automated MODIS Vegetation Continuous Fields (MOD44B) at 250 m Spatial Resolution for Data Years Beginning Day 65, 2000 - 2010, Collection 5 Percent Tree Cover. Available online: http://www.landcover.org/data/vcf/ (accessed 10 June, 2014); 2011.

Elvidge, C. D.; Tuttle, B. T.; Sutton, P. C.; Howard, A. T.; Milesi, C. Global distribution and density of constructed impervious surfaces. Sensors. 7:1962–1979; 2007

Fast, J.D.; Gustafson, W.I.; Chapman, E.G.; Easter, R.C.; Rishel, J.P.; Zaveri, R.A.; Grell, G.A.; Barth, M.C. The Aerosol Modeling Testbed: A Community Tool to Objectively Evaluate Aerosol Process Modules. Bulletin of the American Meteorological Society. 92:343-360; 2011

Geoscience Australia. 1 second SRTM Derived Products User Guide. Available online: http://www.ga.gov.au/corporate_data/72759/1secSRTM_Derived_DEMs_UserGuide_v1.0.4.pdf (accessed June 10, 2014); 2011

Grell, G.A.; Peckham, S.E.; Schmitz, R.; McKeen, S.A.; Frost, G.; Skamarock, W.C.; Eder, B. Fully coupled "online" chemistry within the WRF model. Atmospheric Environment. 39:6957-6975; 2005

Hystad, P.; Setton, E.; Carvantes, A.; Poplawski, K.; Deschenes, S.; Brauer, M., et al. Creating National Air Pollution Models for Population Exposure Assessment in Canada. Environ Health Perspect. 119:1123-1129; 2011

Lamsal, L.N.; Martin, R.V.; van Donkelaar, A.; Steinbacher, M.; Celarier, E.A.; Bucsela, E.; Dunlea, E.J.; Pinto, J.P. Ground-level nitrogen dioxide concentrations inferred from the satellite-borne Ozone Monitoring Instrument. Journal of Geophysical Research: Atmospheres. 113:D16308; 2008

Lamsal, L.N.; Martin, R.V.; van Donkelaar, A.; Celarier, E.A.; Bucsela, E.J.; Boersma, K.F., et al. Indirect validation of tropospheric nitrogen dioxide retrieved from the OMI satellite instrument: Insight into the seasonal variation of nitrogen oxides at the northern midlatitudes. J Geophys Res. 115:D05302; 2010

Levelt, P.F.; Van den Oord, G.H.J.; Dobber, M.R.; Malkki, A.; Huib, V.; de Vries, J.; Stammes, P.; Lundell, J.O.V.; Saari, H. The ozone monitoring instrument. Geoscience and Remote Sensing, IEEE Transactions on. 44:1093-1101; 2006

Novotny, E.V.; Bechle, M.J.; Millet, D.B.; Marshall, J.D. National Satellite-Based Land-Use Regression: NO_2 in the United States. Environmental Science & Technology. 45:4407-4414; 2011

Public Sector Mapping Agencies (PSMA). Transport and Topography Data Product Description. Available online: http://www.psma.com.au/psma/wp-

content/uploads/Transport-and-Topography-Product-Description.pdf (accessed 10 June, 2014); 2013

Olivier, J.G.J.; Van Aardenne, J.A.; Dentener, F.J.; Pagliari, V.; Ganzeveld, L.N.; Peters, J.A.H.W. Recent trends in global greenhouse gas emissions:regional trends 1970–2000 and spatial distributionof key sources in 2000. Environmental Sciences. 2:81-99; 2005

Rose, N.; Cowie, C.; Gillett, R.; Marks, G.B. Validation of a Spatiotemporal Land Use Regression Model Incorporating Fixed Site Monitors. Environmental Science & Technology. 45:294-299; 2011

Schell, B.; Ackermann, I.J.; Hass, H.; Binkowski, F.S.; Ebel, A. Modeling the formation of secondary organic aerosol within a comprehensive air quality model system. J Geophys Res. 106:28275-28293; 2001

Sturman, A.; Tapper, N. The Weather and Climate of Australia and New Zealand: Oxford University Press; 2006

Torres, O.; Tanskanen, A.; Veihelmann, B.; Ahn, C.; Braak, R.; Bhartia, P.K.; Veefkind, P.; Levelt, P. Aerosols and surface UV products from Ozone Monitoring Instrument observations: An overview. Journal of Geophysical Research. 112:1-14; 2007

Tuccella, P.; Curci, G.; Visconti, G.; Bessagnet, B.; Menut, L.; Park, R.J. Modeling of gas and aerosol with WRF/Chem over Europe: Evaluation and sensitivity study. J Geophys Res. 117:D03303; 2012

Webster, R.; Oliver, M.A. Geostatistics for Environmental Scientists: John Wiley and Sons; 2007